Molecular Therapy
Original Article

A SARS-CoV-2 targeted siRNA-nanoparticle therapy for COVID-19

Adi Idris,[1,5] Alicia Davis,[2,3,5] Aroon Supramaniam,[1,5] Dhruba Acharya,[1] Gabrielle Kelly,[1] Yaman Tayyar,[1] Nic West,[1] Ping Zhang,[1] Christopher L.D. McMillan,[4] Citradewi Soemardy,[2] Roslyn Ray,[2] Denis O'Meally,[2] Tristan A. Scott,[2] Nigel A.J. McMillan,[1] and Kevin V. Morris[1,2]

[1]Menzies Health Institute Queensland, School of Medical Science Griffith University, Gold Coast Campus, QLD 4222, Australia; [2]Center for Gene Therapy, Hematological Malignancy and Stem Cell Transplantation Institute at the City of Hope and City of Hope Beckman Research Institute, 1500 E. Duarte Road, Duarte, CA 91010, USA; [3]Irell & Manella Graduate School of Biological Sciences at the City of Hope, Duarte, CA 91010, USA; [4]School of Chemistry and Molecular Biosciences, The University of Queensland, St Lucia, QLD, Australia

Coronavirus disease 2019 (COVID-19) is caused by severe acute respiratory syndrome coronavirus 2 (SARS-CoV-2) infection in humans. Despite several emerging vaccines, there remains no verifiable therapeutic targeted specifically to the virus. Here we present a highly effective small interfering RNA (siRNA) therapeutic against SARS-CoV-2 infection using a novel lipid nanoparticle (LNP) delivery system. Multiple siRNAs targeting highly conserved regions of the SARS-CoV-2 virus were screened, and three candidate siRNAs emerged that effectively inhibit the virus by greater than 90% either alone or in combination with one another. We simultaneously developed and screened two novel LNP formulations for the delivery of these candidate siRNA therapeutics to the lungs, an organ that incurs immense damage during SARS-CoV-2 infection. Encapsulation of siRNAs in these LNPs followed by *in vivo* injection demonstrated robust repression of virus in the lungs and a pronounced survival advantage to the treated mice. Our LNP-siRNA approaches are scalable and can be administered upon the first sign of SARS-CoV-2 infection in humans. We suggest that an siRNA-LNP therapeutic approach could prove highly useful in treating COVID-19 disease as an adjunctive therapy to current vaccine strategies.

INTRODUCTION

Coronaviruses have been previously linked to public health crises including the severe acute respiratory syndrome coronavirus 1 (SARS-CoV-1) outbreak in 2003 and the Middle East Respiratory Coronavirus (MERS-CoV) in 2012. These betacoronaviruses led to approximately 8,096 infections for SARS-CoV-1 and 1,728 infections for MERS (WHO reports, 2004 and 2016, PMID: 27344959). In contrast, the highly transmissible novel SARS-CoV-2 virus quickly escalated to a pandemic with over 128 million cases reported worldwide along with multi-organ failure, acute respiratory distress syndrome, and death in the elderly and in those with underlying morbidities. The race to develop a SARS-CoV-2 vaccine began swiftly and is ongoing; however, the emergence of viral variants has demonstrated the limited effectiveness of some vaccines to these variants.[1,2] These observations suggest an urgent and unmet need for SARS-CoV-2-specific therapies to treat coronavirus disease 2019 (COVID-19). While Dexamethasone and Remdesivir appear to provide some benefit to COVID-19 patients,[3] a therapeutic targeted to directly inhibit SARS-CoV-2 is lacking.

RNA encodes the genome of coronaviruses, rendering them highly susceptible to RNA interference (RNAi),[4–6] particularly when delivered to the lungs of primates.[7] Small interfering RNAs (siRNAs) are short double-stranded RNA molecules that induce gene silencing at the transcriptional or post-transcriptional level and can be delivered to the lungs through either intranasal or intravenous (i.v.) routes.[8,9] We report here the screening of several siRNAs targeted to highly conserved regions of SARS-CoV-2 that block virus expression and replication. Moreover, we find that the top candidate siRNAs are able to functionally repress virus expression *in vivo* and inhibit the emergence of COVID-19 disease when delivered i.v. using particular lipid nanoparticle (LNP) siRNA formulations.

RESULTS

siRNA targeting SARS-CoV-2

To determine the effectiveness of RNAi to SARS-CoV-2, we designed several siRNAs targeted to the ultra-conserved regions in the RNA-dependent RNA polymerase (RdRp), Helicase (Hel), and 5′ untranslated region (5′ UTR). Ultra-conserved siRNAs that target structurally accessible regions were discovered by (1) characterizing the 29,903 bp RNA genome of SARS-CoV-2 for structural features,[10] (2) sequence conservation,[11] (3) RNA modifications,[12] and (4) the absence of seed sequences in the human transcriptome. We used these data to

Received 14 April 2021; accepted 5 May 2021;
https://doi.org/10.1016/j.ymthe.2021.05.004.

[5]These authors contributed equally

Correspondence: Nigel A.J. McMillan, Menzies Health Institute Queensland, School of Medical Science Griffith University, Gold Coast Campus, QLD 4222, Australia.
E-mail: n.mcmillan@griffith.edu.au
Correspondence: Kevin V. Morris, Menzies Health Institute Queensland, School of Medical Science Griffith University, Gold Coast Campus, QLD 4222, Australia.
E-mail: kmorris@coh.org

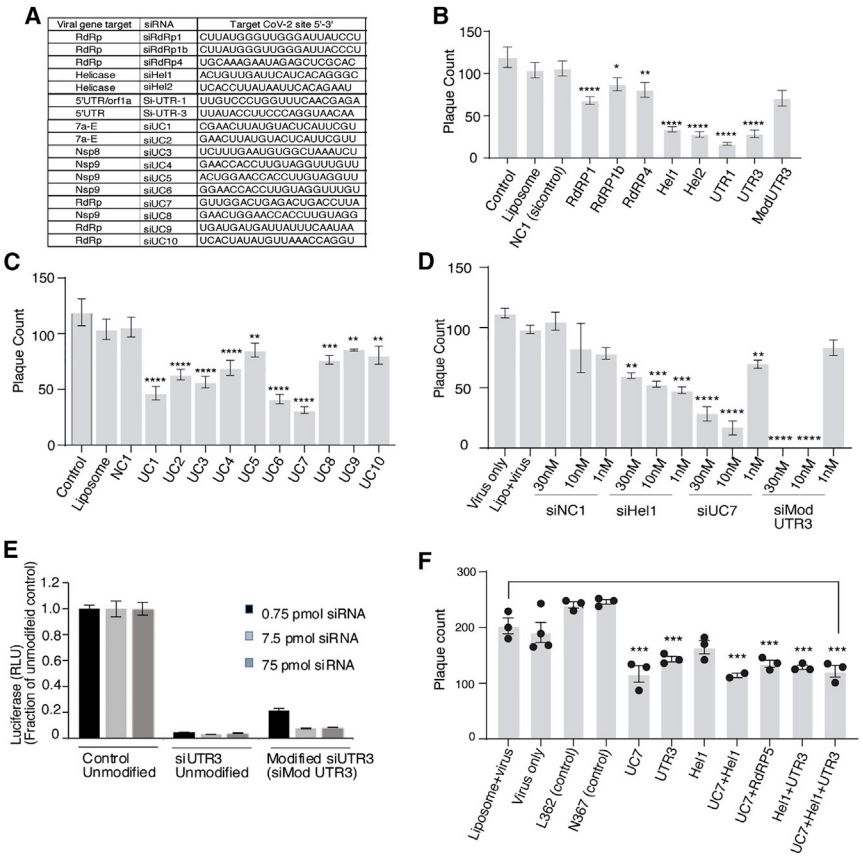

Figure 1. siRNA screening against SARS-CoV-2

(A) The top candidate siRNAs selected for screening against SARS-CoV-2.[16] VeroE6 cells were either pre-treated without (Liposome, Lipo+virus) or with 30 nM of siRNA complexed with Lipofectamine 2000 for 24 h before infection. Viral plaques were counted after 4 days. (B and C) siRNAs targeting genes (B) and phylogenetically conserved regions (C) were tested. (D) The top repressive siRNAs were screened for dose-dependent repression of SARS-CoV-2. (E) The resultant unmodified siRNA controls and the modified siMod UTR3 were transfected with a pSI-Check reporter vector with the 5′ UTR cloned downstream of Renilla luciferase, and knockdown of luciferase activity of the modified siRNA determined relative to the unmodified control. The average of triplicate-treated HEK293 cells is shown with the standard deviation. (F) Combinations of the top candidate siRNAs were selected, mixed in equal molar ratios to a final concentration of 30 nM, and assessed for repression of SARS-CoV-2 *in vitro*. For (B)–(D) and (F), triplicate treated cells are shown with the standard error of the mean of triplicate treatments and *$p < 0.05$,[17] **$p < 0.01$, ***$p < 0.001$, and ****$p < 0.001$ were considered statistically significant as determined by one-way ANOVA analysis (Dunnett's post-test) when compared against virus only (control).

prioritize approximately 9,500 candidate siRNAs generated by OligoWalk[13] and DSIR.[14] In addition, 163 experimentally validated SARS-CoV-1 siRNAs were assessed for homology with SARS-CoV-2. [15] From this stringent bioinformatic approach, 18 siRNAs were selected (Figure 1A; Table S1). The panel of siRNAs screened displayed varying effects on SARS-CoV-2 *in vitro* (Figures 1B and 1C; Figures S1A, S1B, and S1E) with siRNAs Hel1, Hel2, siUC7, and siUTR3 demonstrating the most potent and dose-dependent repression of virus expression (Figure 1D). Candidates siHel1 and siHel2 are within highly conserved regions and are able to target both SARS-CoV-1 and SARS-CoV-2 (Figures S1C and S1D).

Chemical modifications can be used to stabilize siRNAs, which results in a longer-term expression and persistence *in vivo* and generally more potent repression.[18] We selected siUTR3, as this target site resides in stem loop 1, a highly conserved region in the 5′ UTR required for downstream transcriptional processing and expression of several viral RNAs.[19] We find that 2′ O-methyl chemical modifications embedded into siUTR3 (Figure S2) exhibit increased stability in serum (Figure S2) and that repression of SARS-CoV-2 is maintained, although it is less potent than the non-modified siUTR3 (Figures 1B and 1E). We also find that none of the siRNAs tested demonstrated any observable immunostimulatory activity on human macrophages (Figures S3A and S3B).

SARS-CoV-2 is able to rapidly evolve mutations that make the virus refractory to antibody targeting.[1,2,20] It is well known with other RNA viruses, like human immunodeficiency virus (HIV), that single siRNA targeting results in the emergence of viral resistance[21] while combinations of siRNAs have been shown to hamper the emergence of resistant variants.[22] To ascertain whether combining siRNAs can functionally target SARS-CoV-2, we selected and screened three highly repressive siRNAs (siUTR3, siUC7, and siHel1) alone and in combination for repression of virus expression. Interestingly, we find that mixtures of siRNAs offered the same viral knockdown as was observed with single targeted siRNAs, even though the concentration of individual siRNAs in each combination was proportionally lower (50% for two siRNAs and 33% for three siRNAs; Figure 1F). Collectively, these data suggest that siRNAs Hel1, Hel2, siUC7, and siUTR3 either alone or in combination can potently target and repress SARS-CoV-2, that siUTR3 can be chemically modified and retain function, and that these siRNAs do not induce nuclear factor-κB (NF-κB) and interferon regulatory factor (IRF) innate immune activation pathways.

LNP *in vivo* delivery of anti-SARS-CoV-2 siRNAs

Developing therapeutic strategies for viral infections based on siRNAs has so far proved challenging, with poor clinical success primarily being the result of subpar delivery. SARS-CoV-2 infection occurs predominantly in epithelial cells of the respiratory tract and results in diffuse alveolar damage.[23] Macrophage and monocytes are also infected with SARS[24] and may be one source of the observed cytokine storm in COVID-19 disease.[25,26] We previously developed an i.v.

liposome delivery platform that resulted in robust delivery of siRNAs to the lungs *in vivo*.[8,9] Unlike standard liposomes, these "stealth" LNPs (sLNPs) are formulated to be stable in serum, circulate for long periods of time, and to protect siRNA payloads from nucleases. These liposomes can be formulated based on alterations of size and composition to traffic to the lung.[8,9]

Previously published work fully characterized the sLNPs with an average size of 190 nm, polydispersity index of 0.326, zeta potential of 52.1 millivolts (mV), and 94.8% siRNA encapsulation efficiency.[7–9,27,28] Additionally, this work demonstrated that sLNPs can target the lung (~35%), liver (~55%), and spleen (~10%).[8,9] Recent studies have found that increased concentrations of 1,2-dioleoyl-3-trimethylammonium-Propane (DOTAP) with DLin-MC3-DMA (MC3) into the LNP formulations results in enhanced targeting to the lung.[29] As such, we sought to contrast earlier formulated sLNPs containing 50% DOTAP with next generation modified LNPs containing 40% DOTAP+MC3 (dmLNP) for delivery of anti-SARS-CoV-2 siRNAs *in vivo* using the K18-hACE2 mouse model of COVID-19 disease.[16] First, to validate the pathogenicity of SARS-CoV-2 in the K18-hACE2 mouse model, mice were inoculated with 4×10^4 plaque-forming units (PFUs) of virus. Within the first 4 days, dramatic weight loss of ~20% of body weight occurred (Figure S4A) with a corresponding heightened clinical score (Figure S4B). Infected K18-hACE2 mice also exhibited high viral load in the lung (Figure S4C) and brain (Figure S4D), which was infectious upon serial passage (Figure S4E). These data demonstrate, similar to previous observations with SARS-CoV-1,[22,25] that the K18-hACE2 mouse model exhibits COVID-19 disease when infected with SARS-CoV-2.

Next, to determine the ability of the sLNP-siRNAs to functionally repress SARS-CoV-2, K18-hACE2 mice were treated with various sLNP-siRNA formulations i.v. a day before and 2 days after inoculating with 1×10^4 PFU of virus (Figure 2A). We find that sLNP-siRNA treatment provided a survival advantage in the sLNP-siUC7 and sLNP-siHel2 treated mice compared to virus-infected and sLNP-siRNA control treated mice (Figure 2B). The treated mice exhibited less weight loss (Figure 2C) and an overall lower clinical score (Figure 2D) when compared to the control sLNP-siRNA and virus-infected mice. Notably, both the sLNP-siUC7- and sLNP-siHel2-treated mice functionally repressed SARS-CoV-2 *in vivo* at day 3 based on viral outgrowth analysis from lung (Figure 2D), but this effect was lost by day 6, suggesting that the repressive effect of the siRNAs is transient and found ~24–48 h following sLNP-siRNA treatment. Markedly, the siRNA-treated mice appeared most closely aligned with the mock-treated mice when the transcriptomic profile of lung from day 6 was characterized (Figure 2F; Table S2). The sLNP-siRNAs assessed here contain ~50% DOTAP, which is a cationic lipid often used in nanoparticle and liposome formulations. Cationic liposomes can aggregate and lead to accumulation in the spleen, liver, and lung. Notably, the sLNP-siRNA formulations did not appear to exhibit any overt splenomegaly in treated virus-infected mice as determined by post-mortem assessment of the spleens from treated and control animals at day 3 (Figure S5A) and day 6 (Figure S5B) post-treatment. Collectively, these data demonstrate that i.v. injected sLNP-siRNAs can repress SARS-CoV-2 *in vivo* and delay the onset of COVID-19 symptoms and that siHel2 appears to be a potent siRNA for repressing viral expression when delivered i.v. with sLNPs.

The sLNP-siRNAs (Figure 2) contain 50% DOTAP, which contributes to the highly positive surface charge that has been suggested to activate the immune system.[30] To assess the immune stimulatory properties of the sLNP-siRNAs, we assessed mouse lung gene-expression profiles using NanoString immune gene-expression profiling analysis at day 6. Stimulation of interferon-regulated immune genes was observed between mock and virus infected (Figure S6A) and similar patterns of immune gene activation were observed between the virus infected and the various sLNP-siRNA-treated mice (Figures S6B and S6D; Table S3), suggesting that siRNA treatment in these mice was not overtly immune stimulatory.

While we did not observe any notable unique immune dysregulation with the sLNP-siRNAs *in vivo*, and the siRNAs alone did not demonstrate any observable immune stimulation *in vitro* (Figure S3), recent work has suggested that reducing DOTAP can ameliorate LNP-siRNA immune stimulation. Based on these concerns, we screened a panel of formulations with reduced DOTAP at 40%, 35%, and 30% (Figure S7A). Our goal was to develop a next generation "stealth LNP" formulation with reduced DOTAP and in turn incorporate the cationic ionizable lipid MC3 to help facilitate the endosomal release of siRNAs. We observe that our reduced DOTAP LNP formulations range from 80 to 115 nm in size and display low polydispersity values (Figure S7B). The zeta potential of our reduced DOTAP LNP formulations range from 17 to 23 mV (Figure S7C) and there was little observable difference in the zeta potential values between these new formulations despite the stepwise reduction in DOTAP (Figure S7C). Because highly positive surface charges of nanoparticles and liposomes are linked to toxicity,[30] we view our reduction in surface charge as compared to the previous sLNP-siRNA formulation as a favorable step toward reducing potential toxicity. Notably, the sLNPs, which contain a higher positive charge than the dmLNP-siRNAs, did not appear in previous studies to produce any notable toxicities *in vivo*;[8,9,27,28] however, it should be noted that direct comparisons were not carried out here. Furthermore, all formulations in our panel had $\geq$92% encapsulation efficiency of siRNA cargo (Figure S7D) and transmission electron microscope imaging of the DOTAP40 LNPs exhibited a uniform spherical shape (Figure S7E). Remarkably, the DOTAP40 and DOTAP40C LNPs remain stable for at least 9 months when stored at 4°C with nearly 100% retention of encapsulated siRNA (Figures S8A and S8B) and maintains efficient knockdown in psi-Check reporter assay (Figure S8C). Further, DOTAP40C LNPs display activity against an endogenous gene target, Lamin A/C, after 6 days at room temperature or 3 months at 4°C (Figures S8D and S8E). Furthermore, the siRNAs are largely resistant to enzymatic degradation when encapsulated in these LNPs (Figure S9A) and addition of these LNP-siRNAs to primary human macrophages does not alter cell viability (Figure S9B). Based on these observations, we selected the "DOTAP40C" formulation, which contains the highest proportion of MC3 while also retaining a high

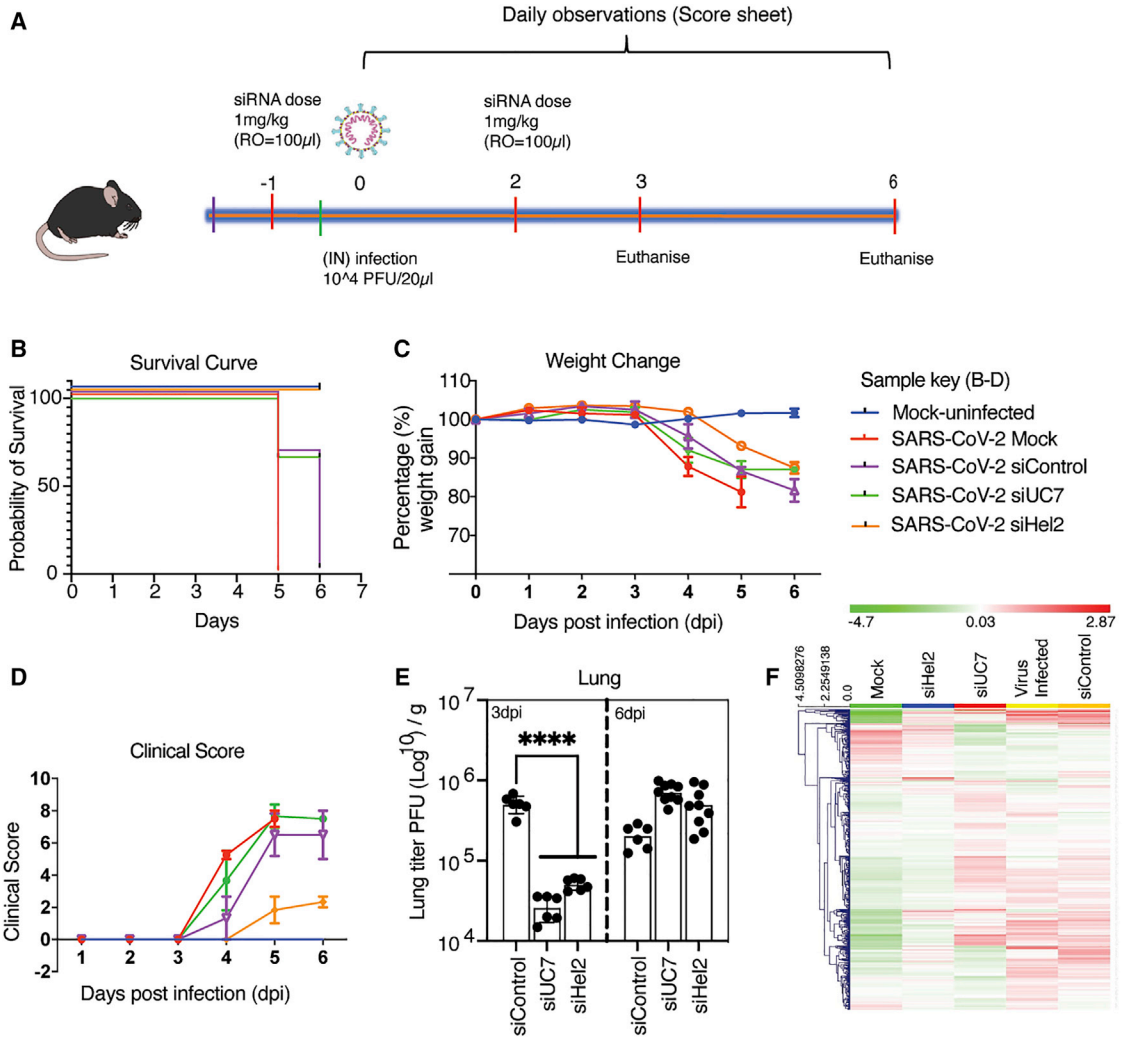

Figure 2. Intravenously administered sLNP-siRNA repression of COVID-19 *in vivo*

(A) 7- and 13-week-old K18-hACE.2 female and male mice were intranasally infected with either PBS or 10^4 PFU/20 μL of SARS-CoV-2 (Australian VIC1 strain, passage 4). (A) Mice (n = 6 for each treatment arm) were intravenously treated with 1 mg/kg in 100 μL of siRNA packaged into hydration of a freeze-dried matrix (HFDM) lipid nanoparticles (LNPs) by retro-orbital administration at −1 and 2 days post infection (dpi). At 3 dpi and 6 dpi lung and brain tissues were harvested and homogenized for immunoplaque assays. (B–D) Mouse survivorship, probability of survival, body weight (weight change), and clinical score were evaluated at the indicated dpi. (B) Weight loss >15% was taken as an endpoint and mice were euthanized. (C) Mice were weighed and scored daily until the experimental end point (6 dpi), for disease progression. (D) The clinical score was evaluated based on locomotion, behavior, and appearance. Each data point represents the average ± SEM of 3 to 4 mice. (E) The amount of infectious virus particles in lung tissues at 3 (n = 2–3 mice) and 6 (n = 2–3 mice) dpi were titrated by immunoplaque assays on Vero E6 cells, using a SARS-CoV-2 N protein-specific antibody and expressed as PFU per gram of tissue. Each data point represents a technical replicate, where one mouse is equivalent to 3 technical replicates and bars represent the average ± SEM. (F) An unsupervised hierarchical cluster heatmap of immune gene expression in the lungs at 6 dpi. Each row is a gene, and each column is a treatment group. Rows are *Z* score normalized (green, low expression and red, high expression). ****$p < 0.0001$ is considered statistically significant when assessed by two-way ANOVA (Dunnett's post-test) when compared against siControl.

proportion of DOTAP, which is important for achieving lung delivery of the candidate SARS-CoV-2 siRNAs. To determine the ability of these newly formulated DOTAP/MP3 LNP-siRNAs (dmLNP-siRNAs, formerly identified as DOTAP40C) to effectively target the lung, we generated DiD labeled dmLNP-siRNA formulations (Figures 3A) and found them to be ∼80 nm (Figure 3B) with a zeta potential of ∼18.58 mV and to encapsulate ≥97% of the control siRNAs (Figure 3C). When injected i.v. into mice and assessed 24 h later, there was localization of DiD fluorescence in the lung (21%), liver (67%), and less so in the spleen (12%; Figures 3D and 3E), which was similar to previous observations with sLNPs.[8,9]

Next, to determine the ability of the dmLNP-siRNAs to deliver functionally repressive siRNAs, K18-hACE2 mice were inoculated with

A

Lipid Component	Molar %
DOTAP	40
MC3	25
DSPC	10
Cholesterol	22
C16-PEG	3

B

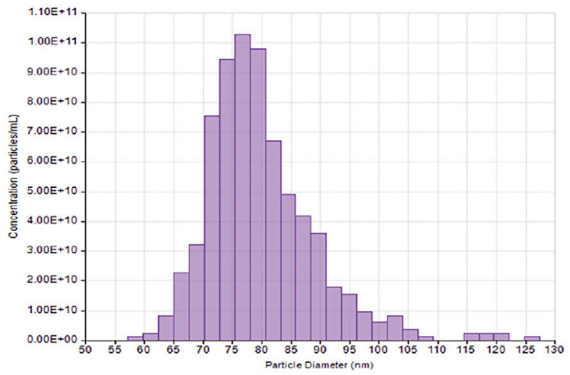

C

Nanoparticle Characteristic	
Average Size	80 nm
Polydispersity (PDI)	0.16
Zeta Potential	18.58 mV
siRNA Encapsulation Efficiency	97.6%

D

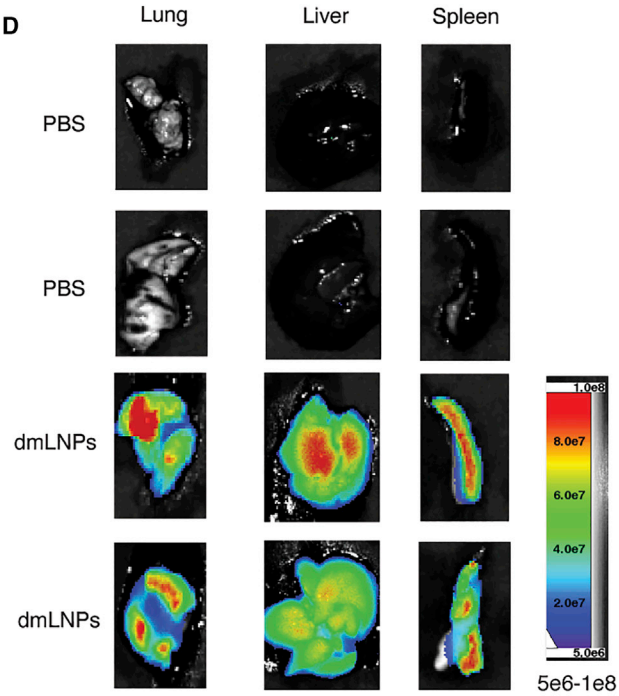

E

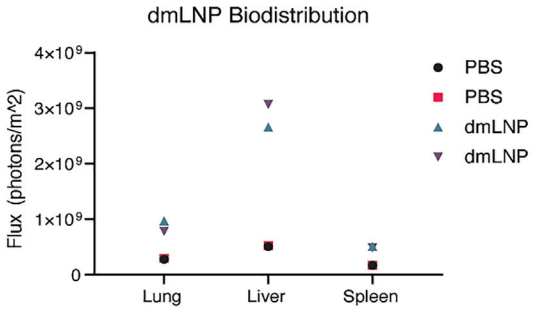

Figure 3. dmLNP-siRNAs characterization and biodistribution

(A) Molar composition of dmLNP-siRNA LNPs. (B) Nanoparticle size distribution of dmLNP-siRNA LNPs was determined using the qNano Gold tuneable resistive pulse sensing device. (C) dmLNP-siRNAnanoparticle characteristics including size, polydispersity (PDI), surface charge (zeta potential), and siRNA encapsulation efficiency. (D) dmLNP-siRNA biodistribution was determined in C57/BL6 mice that received DiD-labeled dmLNP-siRNA nanoparticles at 1 mg/kg siRNA dose or PBS vehicle control via retro-orbital (RO) route. 24 h after injection, mice were euthanized and the lung, liver, and spleen were removed. Organs were imaged for DiD fluorescence using a LagoX small animal imaging machine at excitation and emission wavelength of 640 and 690 nm, respectively. (E) Quantitative analysis of DiD fluorescence in each organ with n = 2 mice per treatment group.

1×10^4 PFU of virus and treated with dmLNP-siRNA formulations (Figure 4A). We find that mice treated with dmLNP-siHel2 exhibited a survival advantage (Figure 4B), less weight-loss (Figure 4C), and a lower clinical score (Figure 4D) when compared to the control dmLNP-siRNA-treated and virus-infected mice. Further, the data showed a recovery of weight and a concomitant decrease in clinical score at days 6–8 in mice treated with dmLNP-siHel2 and dmLNP-siUC7, suggesting that these treatments may alleviate severe disease symptoms. Similar to previous observations with sLNP-siRNA formulations (Figure 2E), both the dmLNP-siUTR3- and dmLNP-siHel2-treated mice functionally repressed SARS-CoV-2 *in vivo* at days 7–8 based on viral outgrowth analysis from lung (Figure 4E) suggesting a bona fide repression of virus *in vivo*. Collectively, these data demonstrate that i.v. injected dmLNP-siRNAs, similar to sLNP-siRNA treatments (Figure 2), repress SARS-CoV-2 *in vivo* and delay the onset of COVID-19 symptoms and that siUC7, siUTR3, and siHel2 appear to be potent siRNAs for repressing viral expression.

DISCUSSION

Currently there are scant antivirals reported that directly target the SARS-CoV-2 RNA genome. Clustered regularly interspaced short palindromic repeats (CRISPR) has recently been used to target SARS-CoV-2,[32] but pre-existing antibodies to CRISPRs[33] and the need to translate the packaged CRISPR mRNA and gRNA in virus

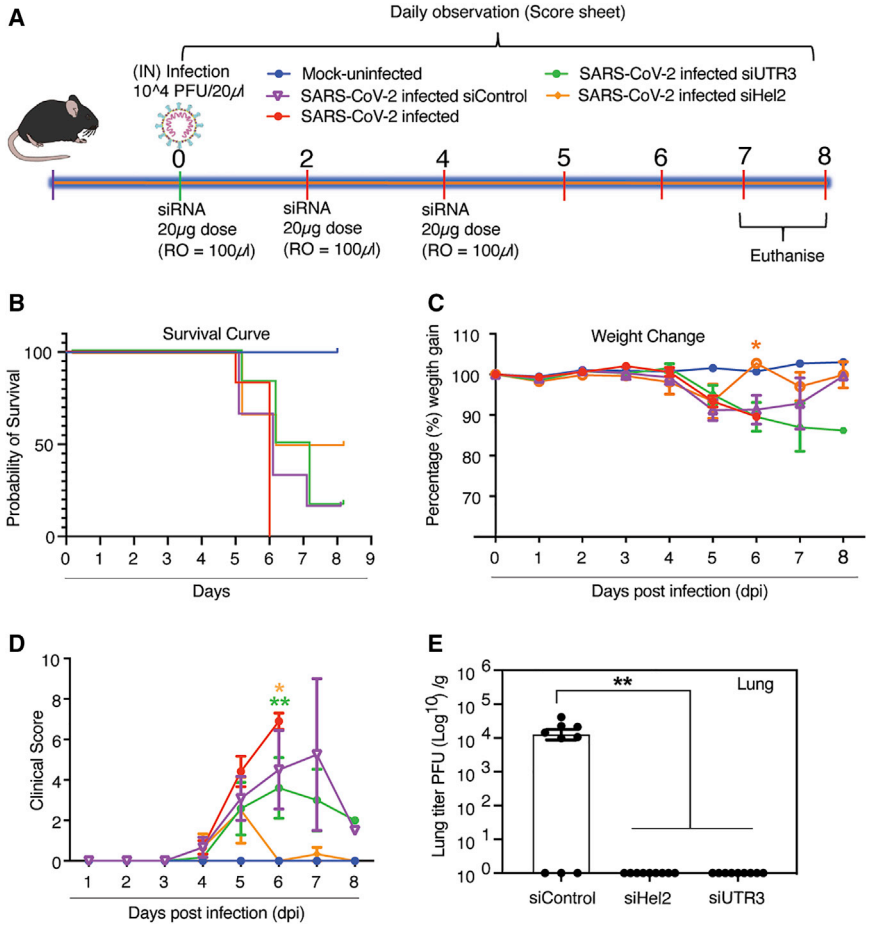

Figure 4. Intravenous administered dmLNP-siRNA suppression of COVID-19 *in vivo*

(A) 7- to 13-week-old K18-hACE2 female and male mice were intranasally infected with either PBS or 1×10^4 PFU/20 μL of SARS-CoV-2 (Australian VIC1 strain, passage 4). (A) Mice (n = 6 for each treatment arm) were i.v. treated with 1 mg/kg in 100 μL of siRNA packaged into DOTAP 40 LNPs by retro-orbital administration at 0, 2, and 4 dpi. At 6–8 dpi, lung tissues were harvested and homogenized for immunoplaque assays. (B–D) Mouse survivorship during infection and dmLNP-siRNA treatment, (B) probability of survival, (C) body weight (weight change), and (D) clinical score were evaluated at the indicated dpi. Mice that lost >15% of their initial body weight were humanely euthanized and plotted as a non-survivor. (B–D) Mice were weighed and scored daily until the experimental endpoint for disease progression. (D) The clinical score was evaluated based on locomotion, behavior, and appearance. Each data point represents the average ± SEM of 3 to 4 mice. (E) The amount of infectious virus particles in lung tissues at 6–8 dpi (n = 3 mice) was determined by immunoplaque assays on Vero E6 cells, using a SARS-CoV-2 N protein-specific antibody and expressed as PFU per gram of tissue. Each data point represents a technical replicate, where one mouse is equivalent to 3 technical replicates and bars represent the average ± SEM $p < 0.05$[17] and $^{**}p < 0.01$ are considered statistically significant when assessed by two-way ANOVA (Dunnett's post-test) against[31] SARS-CoV-2 infected only mice and (E) siControl.

infected cells will hinder the clinical translation of this approach. RNAi does not require translation of mRNA, is programmable, scalable, and stable, and has been observed to potently repress coronaviruses.[4,5,7] We show here that RNAi and particular siRNAs, siHel1, siHel2, UC7, and siUTR3 significantly repress SARS-CoV-2 *in vitro* and *in vivo* and could prove to be a useful therapeutic to treating COVID-19 disease. However, delivery of siRNAs to sites of disease, such as the lungs in COVID-19 afflicted individuals, has remained enigmatic.

The persistent cough and shortness of breath endemic in COVID-19 disease highlight the lungs as a site of significant stress and inflammation during SARS-CoV-2 infection. The thick mucosa associated with COVID-19 will likely impede the delivery of aerosolized therapeutics to infected tissues and additionally, nebulizers increase droplet dispersion, which could lead to infectious particles remaining in the air and thereby increasing the risk of the disease spreading. For these reasons we surmised that an i.v. route of administration as a "backdoor" delivery system might prove both safe and effective. Building on this notion, we turned to "stealth" LNPs,[8,9] which have been shown to deliver siRNAs to the lung, liver, and spleen following an i.v. administration.

Recent work by Cheng et al.[29] demonstrated that LNP formulations can be tuned to specifically target the lung by adjusting the amount of DOTAP incorporated into the particles. Increasing the DOTAP concentration >50% has been reported to result in lung-specific expression of a luciferase mRNA reporter.[29] Notably, this group used a combination of DOTAP (50%) and MC3 (25%) to achieve efficient LNP lung targeting. Our sLNP-siRNAs containing 50% DOTAP and no MC3 target the lung; however, we find the liver and spleen are also targeted.[8,9] Our dmLNP-siRNAs contain 40% DOTAP and 25% MC3, but also display targeting of the lung, liver, and spleen. Notably, the dmLNP-siRNAs (Figures 3 and 4) contained 40% DOTAP and exhibited a concomitant reduction in lung targeting when administered i.v., regardless of the MC3 incorporation, suggesting as others have observed that DOTAP is the key component to targeting the lung with LNPs.[29] DOTAP is a cationic lipid that contributes to the positive surface charge of liposomes and LNPs and has been shown to activate the immune system resulting in systemic toxicity.[34] By reducing the amount of DOTAP in our dmLNP-siRNAs, we have reduced the positive surface charge on the particles by approximately half compared to the sLNP-siRNAs. We also observed some level of immune stimulation that was most likely the result of viral infection and not attributed to the LNP-siRNA formulations as virus-infected controls and LNP-siRNA-particle-treated mice demonstrated a similar gene-expression profile (Figure S6;

Tables S2 and S3). Notably, the siRNA repression of SARS-CoV-2 appeared to be transient, and the effect of viral suppression was lost after ~48 h, suggesting that the LNP-siRNA formulations as a therapeutic will most likely require a daily i.v. regimen during peak viral infection. siRNA modification represents one approach that both reduces immune stimulation and increases the half-life of the siRNAs *in vivo*. Our preliminary data suggest that minimal 2′ O-methyl and phosphorothioate modifications are sufficient to increase the stability of the tested siRNA (UTR3) *in vitro*. Further optimization of such modifications will most likely provide a highly potent and stable siRNA for *in vivo* delivery.

The SARS-CoV-2 vaccine race led by Pfizer and Moderna has opened the door for future LNP-based therapies. Both Pfizer and Moderna vaccines (BNT162b2 and mRNA-1273, respectively) contain an mRNA encoding the Spike protein encapsulated in an LNP delivery vehicle. Prior to the pandemic, the only FDA-approved LNP-based therapy was the siRNA-LNP drug Patisiran (Onpattro) used for the treatment of polyneuropathy caused by hereditary transthyretin-mediated amyloidosis.[31] Recent successes in the clinical translation of LNPs portend a new era in nanomedicine, whereby LNPs are now viewed favorably as bona fide and safe delivery vehicles for mRNAs and RNAi. Building on this realized consensus of interpretation, we show here that i.v. administered stealth LNPs can deliver siRNAs as a therapeutic to treat COVID-19. While both RNAi and LNP technologies are relatively new, it is becoming evident that this next generation technology is programmable, scalable, stable, and relatively safe and has much to offer as a therapeutic to specifically target SARS-CoV-2 and treat COVID-19 disease.

SUPPLEMENTAL INFORMATION

Supplemental information can be found online at https://doi.org/10.1016/j.ymthe.2021.05.004.

ACKNOWLEDGMENTS

We thank Mr. Hamish McMath for assistance with the BL3 facility and vivarium at Griffith University. We thank Olga Villamizar, Ryan Urak, and Liliana Echavarria for their assistance with the LNP characterization and animal work at City of Hope, Duarte CA. We would also like to thank Dr. Adam Taylor from the School of Medical Science, Griffith University for assistance with animal work in the PC3 facility. We also thank Dr. Zhuo Li and Ricardo Zerda at City of Hope Electron Microscopy Core Facility for electron microscopy assistance. This work was supported by NIMH R01 113407-01 and NIAID R56 AI147684 to K.V.M., MRFF 2001931 to N.M., and core services at COH supported by the National Cancer Institute of the National Institutes of Health award number P30CA033572.

AUTHOR CONTRIBUTIONS

A.I. and A.S. designed and conducted animal experiments, G.K., D.A., T.A.S., R.R., A.D., and C.S. carried out experiments, D.O., R.R., and T.A.S. designed and characterized the various siRNAs, A.D. designed, optimized, and generated dmLNP-siRNAs, Y.T. generated sLNP-siRNA formulations, N.A.J.M. and K.V.M. conceived, designed the experiments, and wrote the manuscript. All authors have reviewed and edited the manuscript.

DECLARATION OF INTERESTS

K.V.M., A.D., T.A.S., D.O., and R.R. have submitted provisional patent 048440-762P02US on the technologies reported here.

REFERENCES

1. Chen, R.E., Zhang, X., Case, J.B., Winkler, E.S., Liu, Y., VanBlargan, L.A., Liu, J., Errico, J.M., Xie, X., Suryadevara, N., et al. (2021). Resistance of SARS-CoV-2 variants to neutralization by monoclonal and serum-derived polyclonal antibodies. Nat. Med. *27*, 717–726.

2. Wang, P., Liu, L., Iketani, S., Luo, Y., Guo, Y., Wang, M., Yu, J., Zhang, B., Kwong, P.D., Graham, B.S., et al. (2021). Increased Resistance of SARS-CoV-2 Variants B.1.351 and B.1.1.7 to Antibody Neutralization. bioRxiv. https://doi.org/10.1101/2021.01.25.428137.

3. Beigel, J.H., Tomashek, K.M., Dodd, L.E., Mehta, A.K., Zingman, B.S., Kalil, A.C., Hohmann, E., Chu, H.Y., Luetkemeyer, A., Kline, S., et al.; ACTT-1 Study Group Members (2020). Remdesivir for the Treatment of Covid-19 - Final Report. N. Engl. J. Med. *383*, 1813–1826.

4. Wu, C.J., Huang, H.W., Liu, C.Y., Hong, C.F., and Chan, Y.L. (2005). Inhibition of SARS-CoV replication by siRNA. Antiviral Res. *65*, 45–48.

5. Shi, Y., Yang, D.H., Xiong, J., Jia, J., Huang, B., and Jin, Y.X. (2005). Inhibition of genes expression of SARS coronavirus by synthetic small interfering RNAs. Cell Res. *15*, 193–200.

6. Wu, C.J., and Chan, Y.L. (2006). Antiviral applications of RNAi for coronavirus. Expert Opin. Investig. Drugs *15*, 89–97.

7. Li, B.J., Tang, Q., Cheng, D., Qin, C., Xie, F.Y., Wei, Q., Xu, J., Liu, Y., Zheng, B.J., Woodle, M.C., et al. (2005). Using siRNA in prophylactic and therapeutic regimens against SARS coronavirus in Rhesus macaque. Nat. Med. *11*, 944–951.

8. McCaskill, J., Singhania, R., Burgess, M., Allavena, R., Wu, S., Blumenthal, A., and McMillan, N.A. (2013). Efficient Biodistribution and Gene Silencing in the Lung epithelium via Intravenous Liposomal Delivery of siRNA. Mol. Ther. Nucleic Acids *2*, e96.

9. Wu, S.Y., Putral, L.N., Liang, M., Chang, H.I., Davies, N.M., and McMillan, N.A. (2009). Development of a novel method for formulating stable siRNA-loaded lipid particles for in vivo use. Pharm. Res. *26*, 512–522.

10. Andrews, R.J., Peterson, J.M., Haniff, H.S., Chen, J., Williams, C., Grefe, M., Disney, M.D., and Moss, W.N. (2020). An in silico map of the SARS-CoV-2 RNA Structurome. bioRxiv. https://doi.org/10.1101/2020.04.17.045161.

11. Rangan, R., Zheludev, I.N., Hagey, R.J., Pham, E.A., Wayment-Steele, H.K., Glenn, J.S., and Das, R. (2020). RNA genome conservation and secondary structure in SARS-CoV-2 and SARS-related viruses: a first look. RNA *26*, 937–959.

12. Kim, D., Lee, J.Y., Yang, J.S., Kim, J.W., Kim, V.N., and Chang, H. (2020). The Architecture of SARS-CoV-2 Transcriptome. Cell *181*, 914–921.e10.

13. Mathews, D.H. (2010). Using OligoWalk to identify efficient siRNA sequences. Methods Mol. Biol. *629*, 109–121.

14. Vert, J.P., Foveau, N., Lajaunie, C., and Vandenbrouck, Y. (2006). An accurate and interpretable model for siRNA efficacy prediction. BMC Bioinformatics *7*, 520.

15. Thakur, N., Qureshi, A., and Kumar, M. (2012). VIRsiRNAdb: a curated database of experimentally validated viral siRNA/shRNA. Nucleic Acids Res. *40*, D230–D236.

16. Nagata, N., Iwata, N., Hasegawa, H., Fukushi, S., Harashima, A., Sato, Y., Saijo, M., Taguchi, F., Morikawa, S., and Sata, T. (2008). Mouse-passaged severe acute respiratory syndrome-associated coronavirus leads to lethal pulmonary edema and diffuse alveolar damage in adult but not young mice. Am. J. Pathol. *172*, 1625–1637.

17. Leng, Z., Zhu, R., Hou, W., Feng, Y., Yang, Y., Han, Q., Shan, G., Meng, F., Du, D., Wang, S., et al. (2020). Transplantation of ACE2^{-} Mesenchymal Stem Cells Improves the Outcome of Patients with COVID-19 Pneumonia. Aging Dis. *11*, 216–228.

18. Selvam, C., Mutisya, D., Prakash, S., Ranganna, K., and Thilagavathi, R. (2017). Therapeutic potential of chemically modified siRNA: Recent trends. Chem. Biol. Drug Des. *90*, 665–678.

19. Miao, Z., Tidu, A., Eriani, G., and Martin, F. (2021). Secondary structure of the SARS-CoV-2 5′-UTR. RNA Biol. *18*, 447–456.

20. Weisblum, Y., Schmidt, F., Zhang, F., DaSilva, J., Poston, D., Lorenzi, J.C., Muecksch, F., Rutkowska, M., Hoffmann, H.H., Michailidis, E., et al. (2020). Escape from neutralizing antibodies by SARS-CoV-2 spike protein variants. eLife *9*, e61312.

21. Das, A.T., Brummelkamp, T.R., Westerhout, E.M., Vink, M., Madiredjo, M., Bernards, R., and Berkhout, B. (2004). Human immunodeficiency virus type 1 escapes from RNA interference-mediated inhibition. J. Virol. *78*, 2601–2605.

22. Liu, Y.P., Haasnoot, J., ter Brake, O., Berkhout, B., and Konstantinova, P. (2008). Inhibition of HIV-1 by multiple siRNAs expressed from a single microRNA polycistron. Nucleic Acids Res. *36*, 2811–2824.

23. Hu, B., Guo, H., Zhou, P., and Shi, Z.L. (2021). Characteristics of SARS-CoV-2 and COVID-19. Nat. Rev. Microbiol. *19*, 141–154.

24. Yilla, M., Harcourt, B.H., Hickman, C.J., McGrew, M., Tamin, A., Goldsmith, C.S., Bellini, W.J., and Anderson, L.J. (2005). SARS-coronavirus replication in human peripheral monocytes/macrophages. Virus Res. *107*, 93–101.

25. Channappanavar, R., and Perlman, S. (2017). Pathogenic human coronavirus infections: causes and consequences of cytokine storm and immunopathology. Semin. Immunopathol. *39*, 529–539.

26. McCray, P.B., Jr., Pewe, L., Wohlford-Lenane, C., Hickey, M., Manzel, L., Shi, L., Netland, J., Jia, H.P., Halabi, C., Sigmund, C.D., et al. (2007). Lethal infection of K18-hACE2 mice infected with severe acute respiratory syndrome coronavirus. J. Virol. *81*, 813–821.

27. Khairuddin, N., Blake, S.J., Firdaus, F., Steptoe, R.J., Behlke, M.A., Hertzog, P.J., and McMillan, N.A. (2014). In vivo comparison of local versus systemic delivery of immunostimulating siRNA in HPV-driven tumours. Immunol. Cell Biol. *92*, 156–163.

28. Wu, S.Y., Chang, H.I., Burgess, M., and McMillan, N.A. (2011). Vaginal delivery of siRNA using a novel PEGylated lipoplex-entrapped alginate scaffold system. J. Control. Release *155*, 418–426.

29. Cheng, Q., Wei, T., Farbiak, L., Johnson, L.T., Dilliard, S.A., and Siegwart, D.J. (2020). Selective organ targeting (SORT) nanoparticles for tissue-specific mRNA delivery and CRISPR-Cas gene editing. Nat. Nanotechnol. *15*, 313–320.

30. Xue, H.Y., Liu, S., and Wong, H.L. (2014). Nanotoxicity: a key obstacle to clinical translation of siRNA-based nanomedicine. Nanomedicine (Lond.) *9*, 295–312.

31. Kristen, A.V., Ajroud-Driss, S., Conceição, I., Gorevic, P., Kyriakides, T., and Obici, L. (2019). Patisiran, an RNAi therapeutic for the treatment of hereditary transthyretin-mediated amyloidosis. Neurodegener. Dis. Manag. *9*, 5–23.

32. Blanchard, E.L., Vanover, D., Bawage, S.S., Tiwari, P.M., Rotolo, L., Beyersdorf, J., Peck, H.E., Bruno, N.C., Hincapie, R., Michel, F., et al. (2021). Treatment of influenza and SARS-CoV-2 infections via mRNA-encoded Cas13a in rodents. Nat. Biotechnol.

33. Charlesworth, C.T., Deshpande, P.S., Dever, D.P., Camarena, J., Lemgart, V.T., Cromer, M.K., Vakulskas, C.A., Collingwood, M.A., Zhang, L., Bode, N.M., et al. (2019). Identification of preexisting adaptive immunity to Cas9 proteins in humans. Nat. Med. *25*, 249–254.

34. Kedmi, R., Ben-Arie, N., and Peer, D. (2010). The systemic toxicity of positively charged lipid nanoparticles and the role of Toll-like receptor 4 in immune activation. Biomaterials *31*, 6867–6875.

YMTHE, Volume *29*

Supplemental Information

A SARS-CoV-2 targeted siRNA-nanoparticle therapy for COVID-19

Adi Idris, Alicia Davis, Aroon Supramaniam, Dhruba Acharya, Gabrielle Kelly, Yaman Tayyar, Nic West, Ping Zhang, Christopher L.D. McMillan, Citradewi Soemardy, Roslyn Ray, Denis O'Meally, Tristan A. Scott, Nigel A.J. McMillan, and Kevin V. Morris

Supplemental Figures

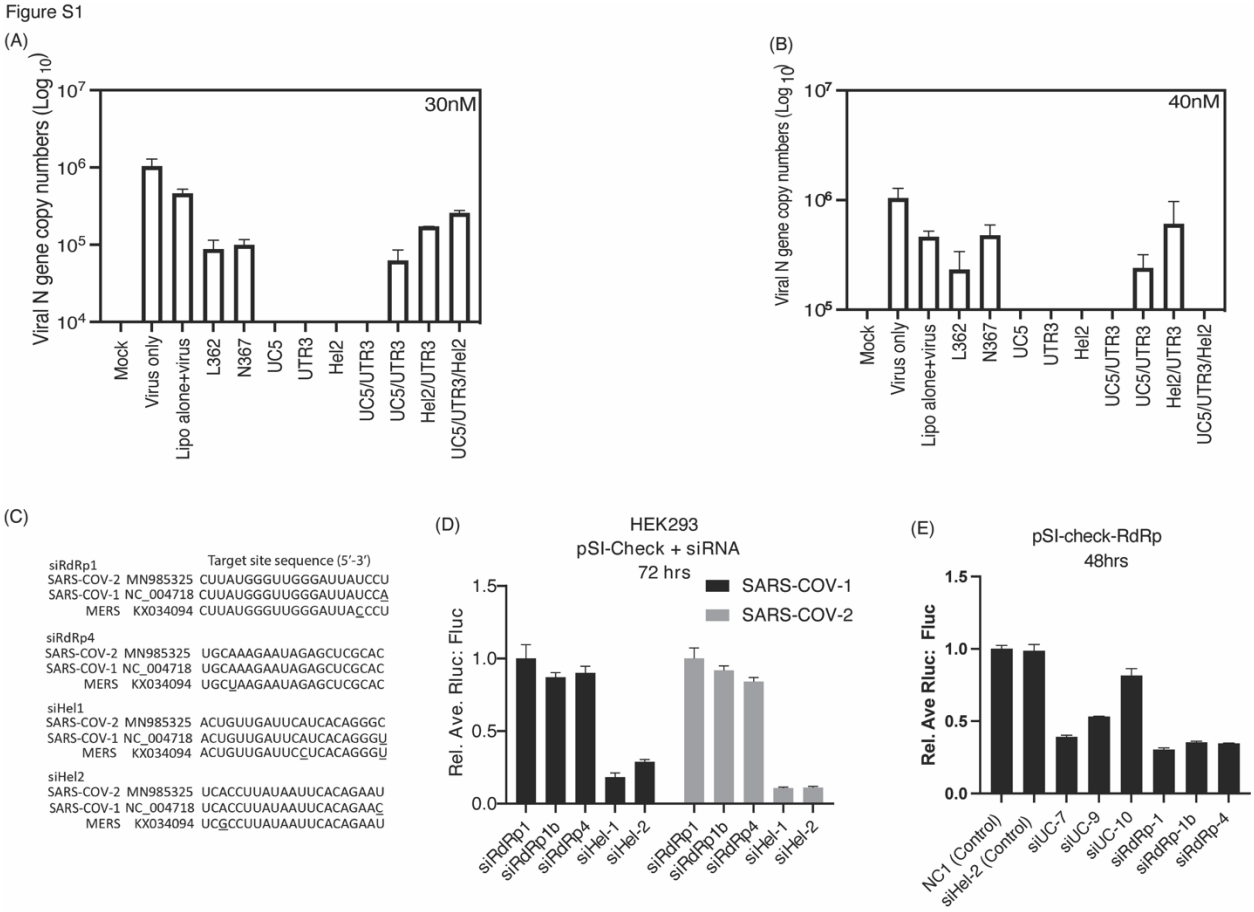

Figure S1 *SiRNA-mediated knockdown of conserved beta-coronavirus sites in the helicase ORF. VeroE6 cells were either untreated [1], pre-treated without (Lipo alone+virus) or with siRNA complexed with Lipofectamine 2000 for 24 hours before infection. Combinations of the siRNAs were selected, mixed in equal molar ratios to a final concentration of either (**A**) 30nM or (**B**) 40nM and viral copy numbers were determined by digital droplet PCR against the N gene at 4dpi. Data is representative of the range of the mean of duplicate treatments. (**C**) siRNA target site conservation between various beta coronaviruses. Alignments are shown between SARS-CoV-1, SARS-CoV-2 and MERs. Underlined DNA bases indicate a different nucleotide compared to SARS-CoV-2. **(D)** A reporter vector containing the helicase ORF for SARS-CoV-1 and SARS-CoV-2 inserted downstream of Renilla luciferase (Rluc) was transfected with siRNAs targeting RdRp (siRdRp1,1b and 4) and helicase (siHel-1 and 2). (**E**) A pSi-Check reporter vector containing the RdRp ORF from SARS-COV-2 was inserted downstream of Renilla luciferase (Rluc) and was transfected with their cognate siRNAs. For (D-E) The levels of RLuc activity were assessed at 72 hrs post-transfection, normalized to background firefly luciferase (Fluc) levels and made relative to a control siRNA, which was used as a negative control and set at 100%. The error bars represent standard deviation from transfections performed in triplicate.*

Figure S2

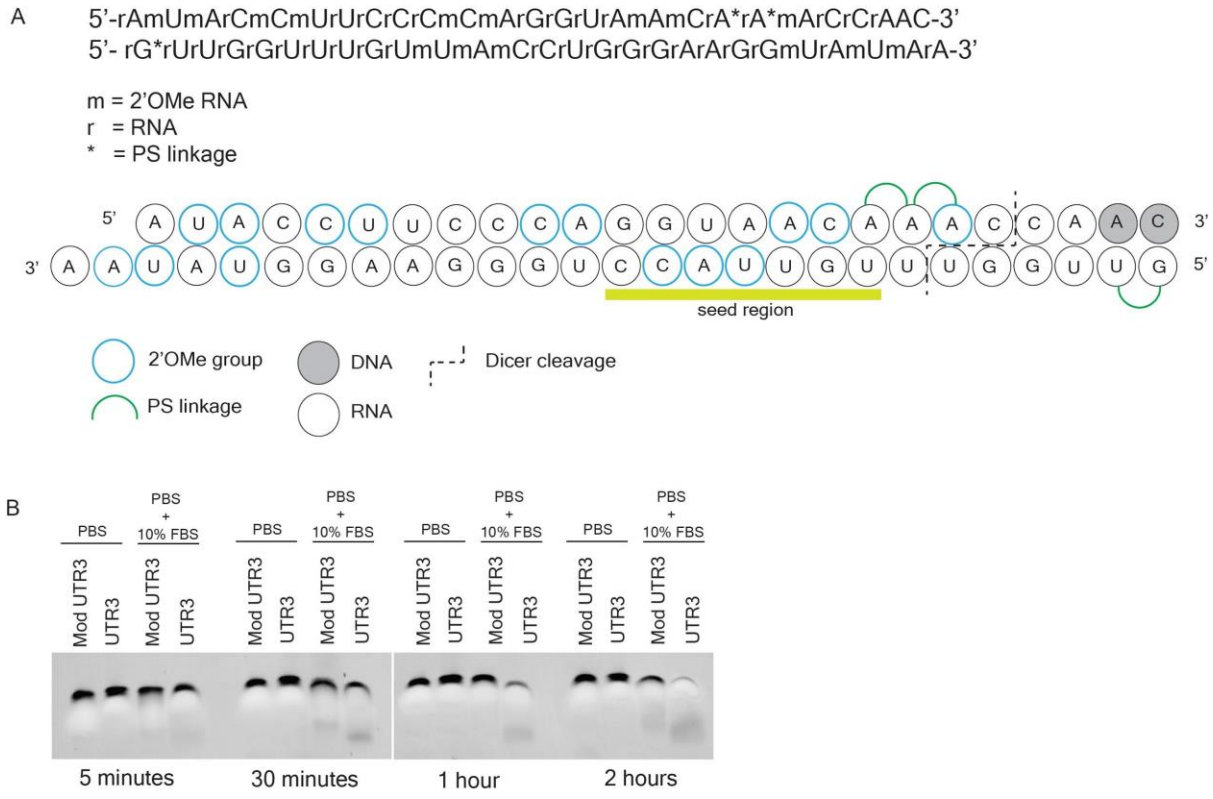

Figure S2 *Chemical modifications imbued in dsiUTR3. (**A**) The dsiRNA UTR3 (siMod UTR3) is shown with the chemical modifications utilized to stabilize the dsiRNA and (**B**) enhance persistence while inhibiting immunogenicity. Modifications were primarily located at CA or CU regions, as these are most sensitive to nuclease activity. Phosphorothioate bonds were used to prevent nuclease activity and to decrease thermostability. This was preferentially done on the passenger strand at positions 19 and 20, to decrease thermostability at the 3' end and thus promote loading of the antisense strand into the RISC complex (35). (**B**) The serum stability assay indicates the modified dsiRNA is substantially protected from nuclease attack compared to its unmodified counterpart. The assay was performed with 10 μM modified and unmodified dsiRNA in 1 X PBS or 1X PBS supplemented with 10% FBS (not heat inactivated). Samples were incubated at 37°C for 5 min, 0.5, 1 and 2 hr time points and electrophoresed on a 6% TBE polyacrylamide gel (Novex, Invitrogen) for 30 min at 180V. Samples were stained with 2 μg/mL EtBr and images acquired under 254 nm using an EZ Imager (Bio-Rad).*

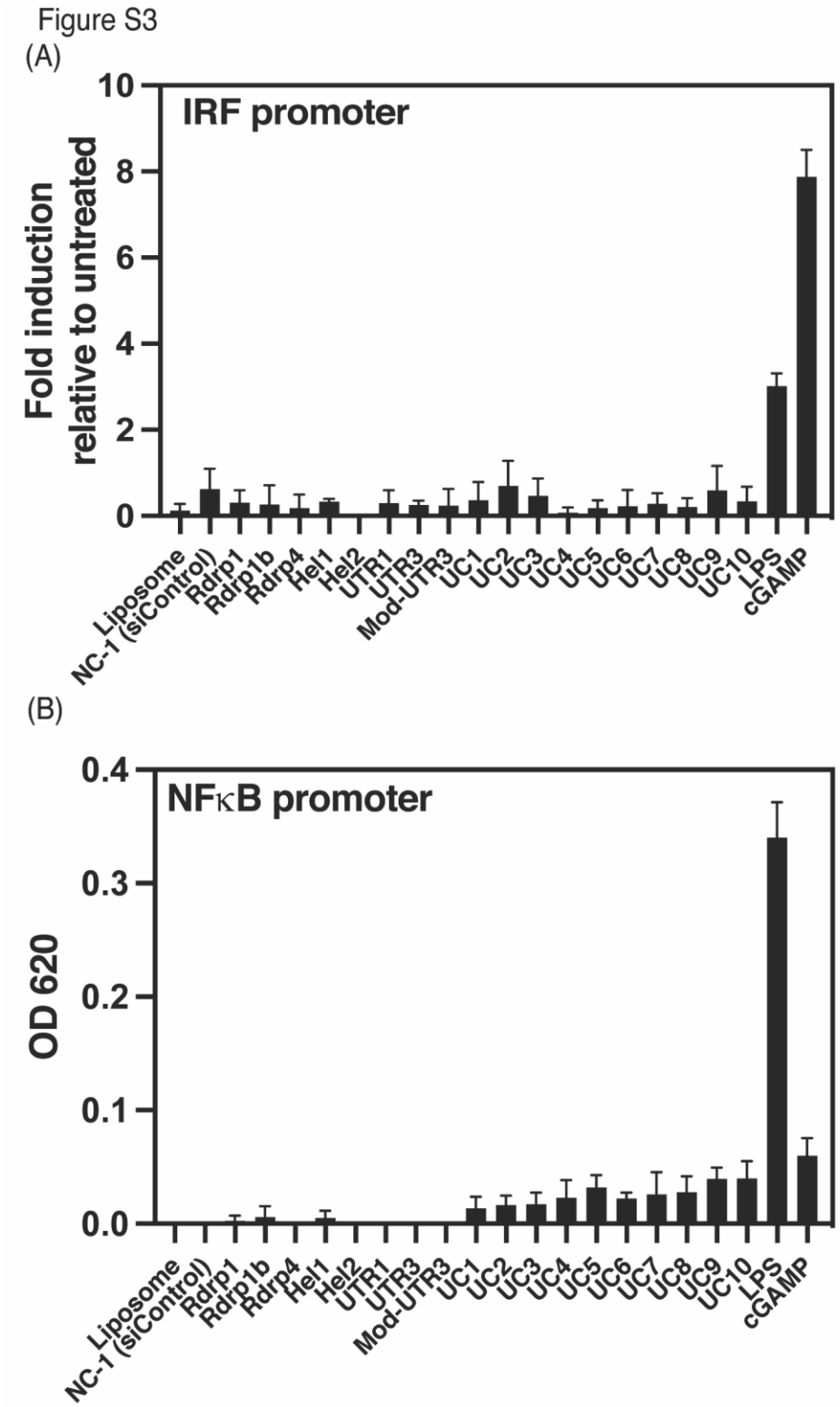

Figure S3 *Immunostimulatory nature of SAR-COV-2 targeted siRNAs. (**A**-**B**) THP-1 DUAL cells, a well-recognized standard to measure immunostimulation, were transfected with indicated siRNAs using Fugene 6 for 24h before quantifying for (**A**) IRF and (**B**) NFkB gene reporter*

expression. Error bars denote SEM of triplicate treatments. 2'3'-cGAMP (20µg/ml) and LPS (100ng/ml) were used as positive controls for IRF and NFkB pathway stimulation, respectively.

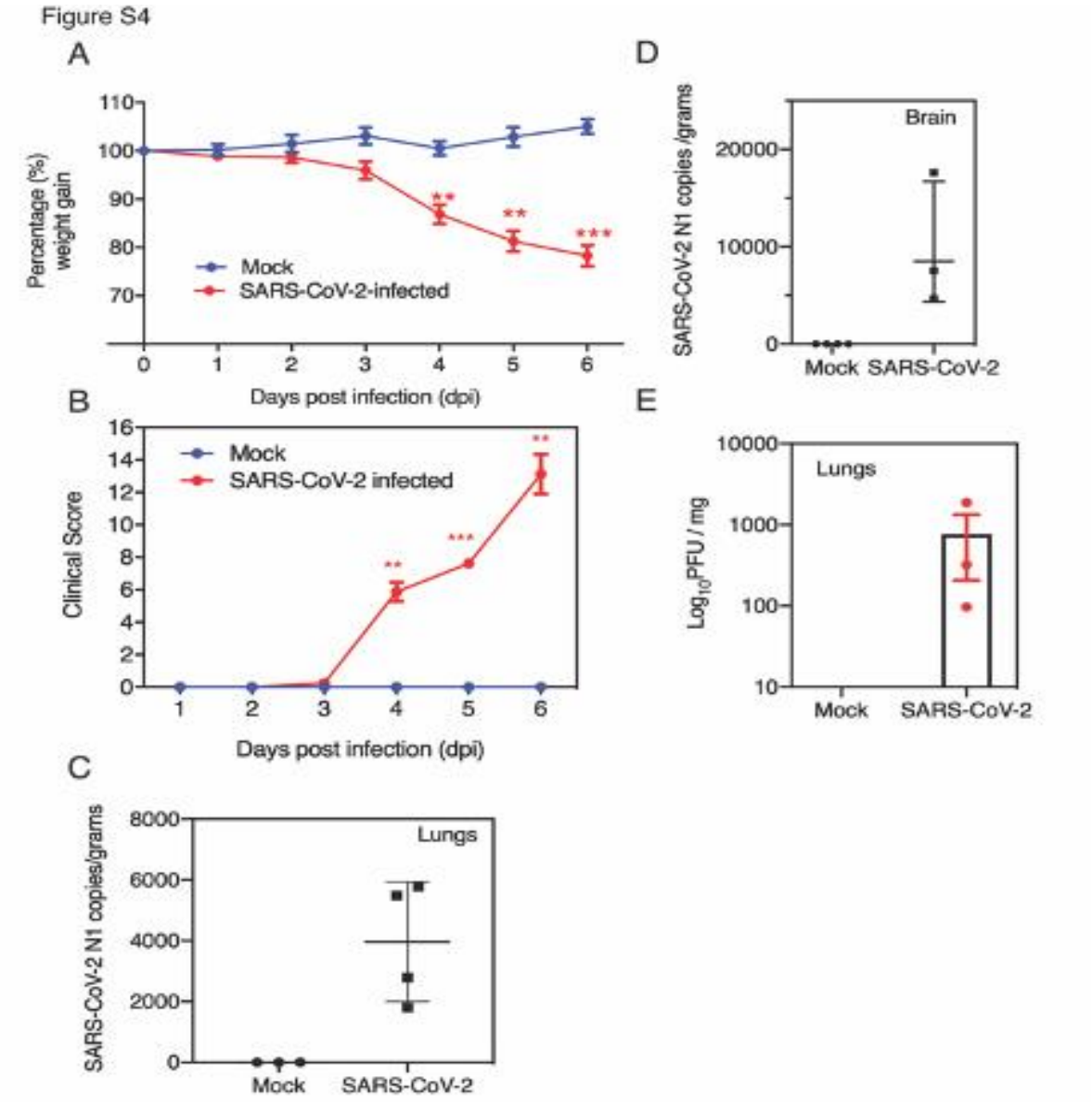

Figure S4 *SARS-CoV-2 infection resulted in severe clinical disease and weight loss in vivo. K18-hACE2 female and male mice, 7–13-week-old, were intranasally infected with either PBS (36) or 4 x 10^4 PFU/ 20 µL of SARS-CoV-2 (Australian VIC1 strain, passage 4). (**A-B**) Mice (n=3-4 for each treatment arm) were weighed and scored daily until the experimental endpoint, for disease progression. (**B**) The clinical score was evaluated based on locomotion, behaviour and appearance. (**C-E**) At 6dpi lung and brain tissues were harvested and homogenized for immunoplaque assays and RNA extracted for viral copy number determination. (33) Viral copy numbers in lung and brain tissues were determined by digital droplet PCR against the N gene and expressed as viral copies per gram of tissue. (**E**) Infectious viral load in lung tissues were*

*determined by immunoplaque assays on Vero E6 cells, using a SARS-CoV-2 N protein specific antibody and expressed as PFU per gram of tissue. (**A-B**) Each data point represents the average ± SEM of 3 to 4 mice. (**C-E**) Each data point represents an individual mouse and bars or lines represent the average ± SEM. (**A-E**) P values of <0.05 (27), <0.01 (**) and <0.001 (***) are considered statistically significant when assessed by Student t- test against mock control.*

Figure S5

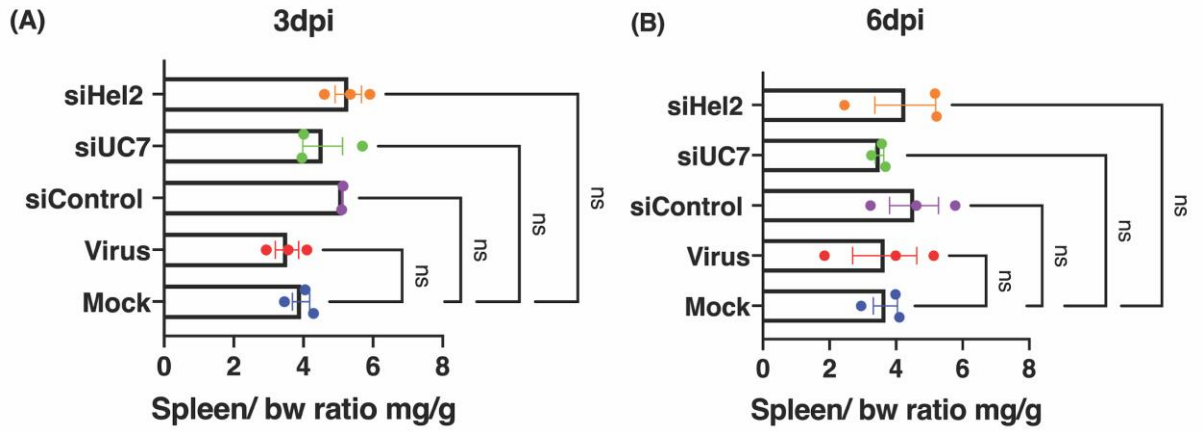

Figure S5 *Retro-orbitally administered LNP-siRNA treatment maintained normal spleen to body weight ratios in treated mice. K18-hACE2 female and male mice, 7–13-week-old, were intranasally infected with either PBS (36) or 1x10^4 PFU/ 20 µL of SARS-CoV-2 (Australian VIC1 strain, passage 4). Mice were retro-orbitally (RO) treated with 1mg/kg in 100 µL of siRNA packaged into HFDM lipid nanoparticles (LNP) at days -1 and 2 post infection. (**A-B**) Mice were sacrificed at (**A**) 3 dpi (n=3 mice) and (**B**) 6 dpi (n=3 mice) and relative organ/body weight ratios of spleen was graphed. Each data point represents an individual mouse and bars represent the average ± SEM.*

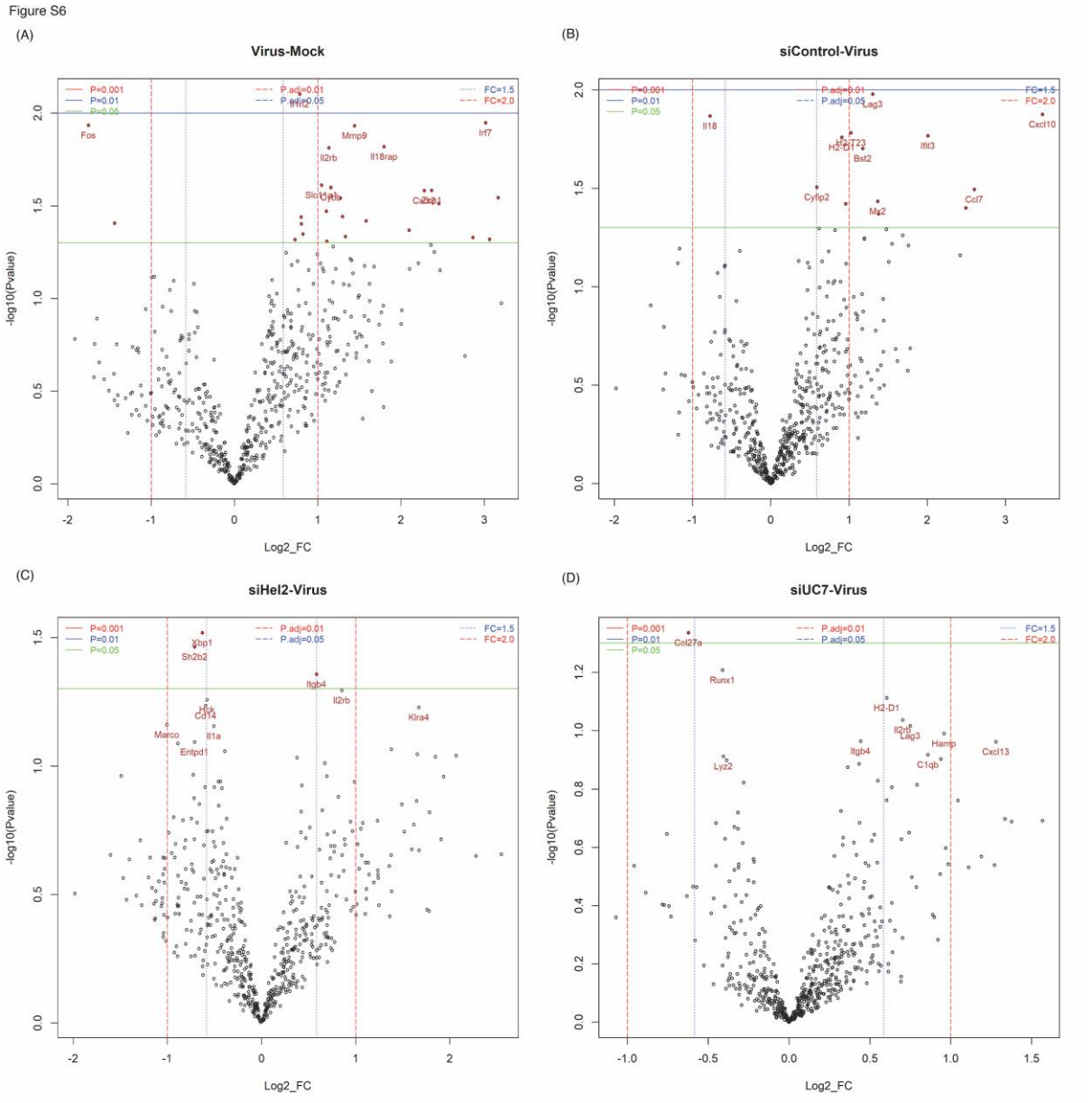

Figure S6 *Volcano plots of differentially expressed immune genes in the lungs of K18-hACE2 female and male mice, 7–13-week-old, intranasally (IN) infected with either PBS (36), 10^4 PFU/ 20 µL of SARS-CoV-2 or SARS-CoV-2 and siRNA treatment. (**A**) Virus alone vs. Mock, (**B**) siControl vs. Virus alone, (**C**) Virus alone vs. siHel2 treated and (**D**) Virus alone vs. siUC7 treated from day 6. Refer to Table S3 for raw data. Data is representative of one mouse per treatment arm.*

Figure S7

(A)

Formulation Name	DOTAP	MC3	DSPC	Cholesterol	C16 PEG
DOTAP 40	40	10	10	37	3
DOTAP 35	35	15	10	37	3
DOTAP 30	30	20	10	37	3
DOTAP 40C	40	25	10	22	3

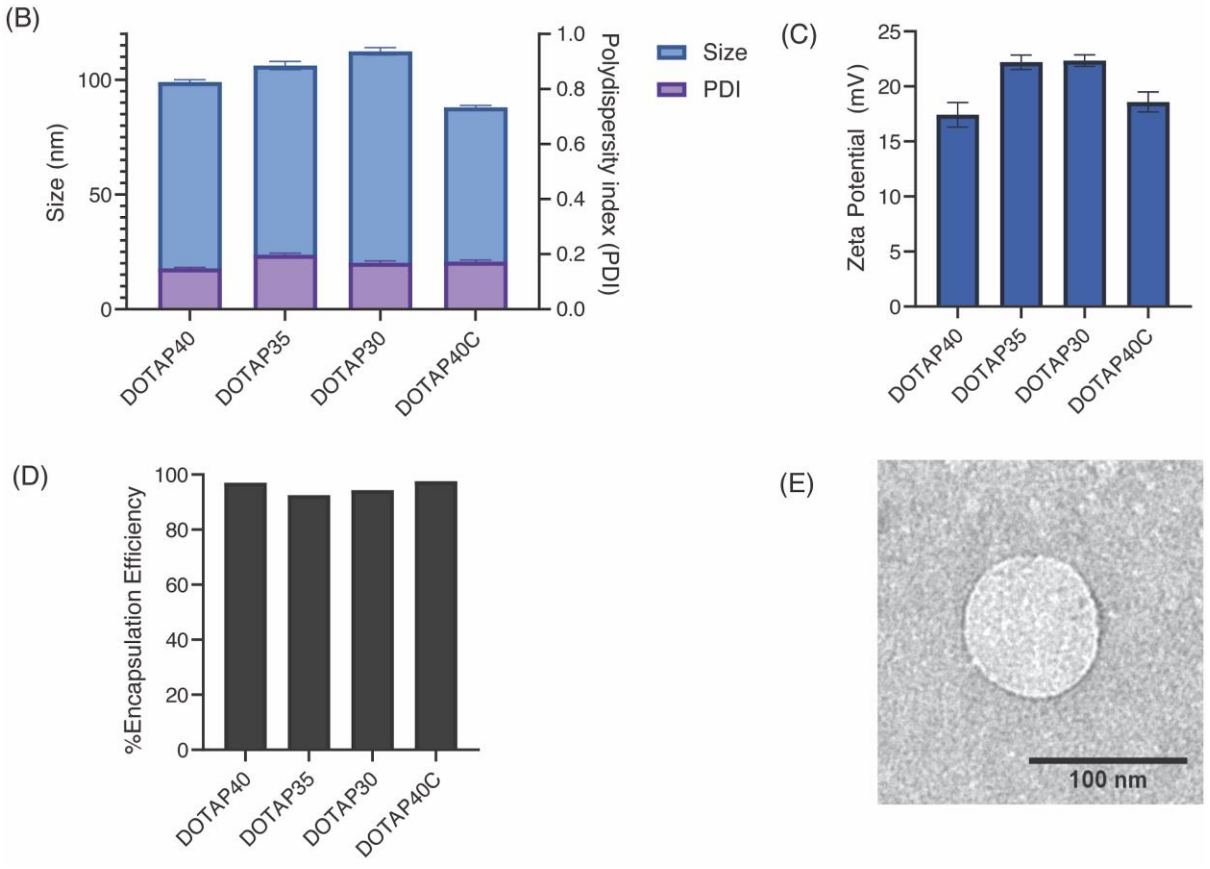

Figure S7 *Optimization of reduced DOTAP nanoparticle formulations. (**A**) Composition of DOTAP nanoparticle formulations with Molar% of each lipid component reported. (**B**) Average size and polydispersity index of each DOTAP formulation was determined by dynamic light scattering (DLS). Error bars represent the S.E.M. of 5 runs (**C**) Average zeta potential reported in millivolts (mV) for each DOTAP formulation. Error bars represent the S.E.M. of 10 runs (**D**) SiRNA encapsulation efficiency of each formulation was determined using the Quant-IT Ribogreen assay. (**E**) Representative transmission electron microscope (TEM) image of DOTAP 40 nanoparticle formulation.*

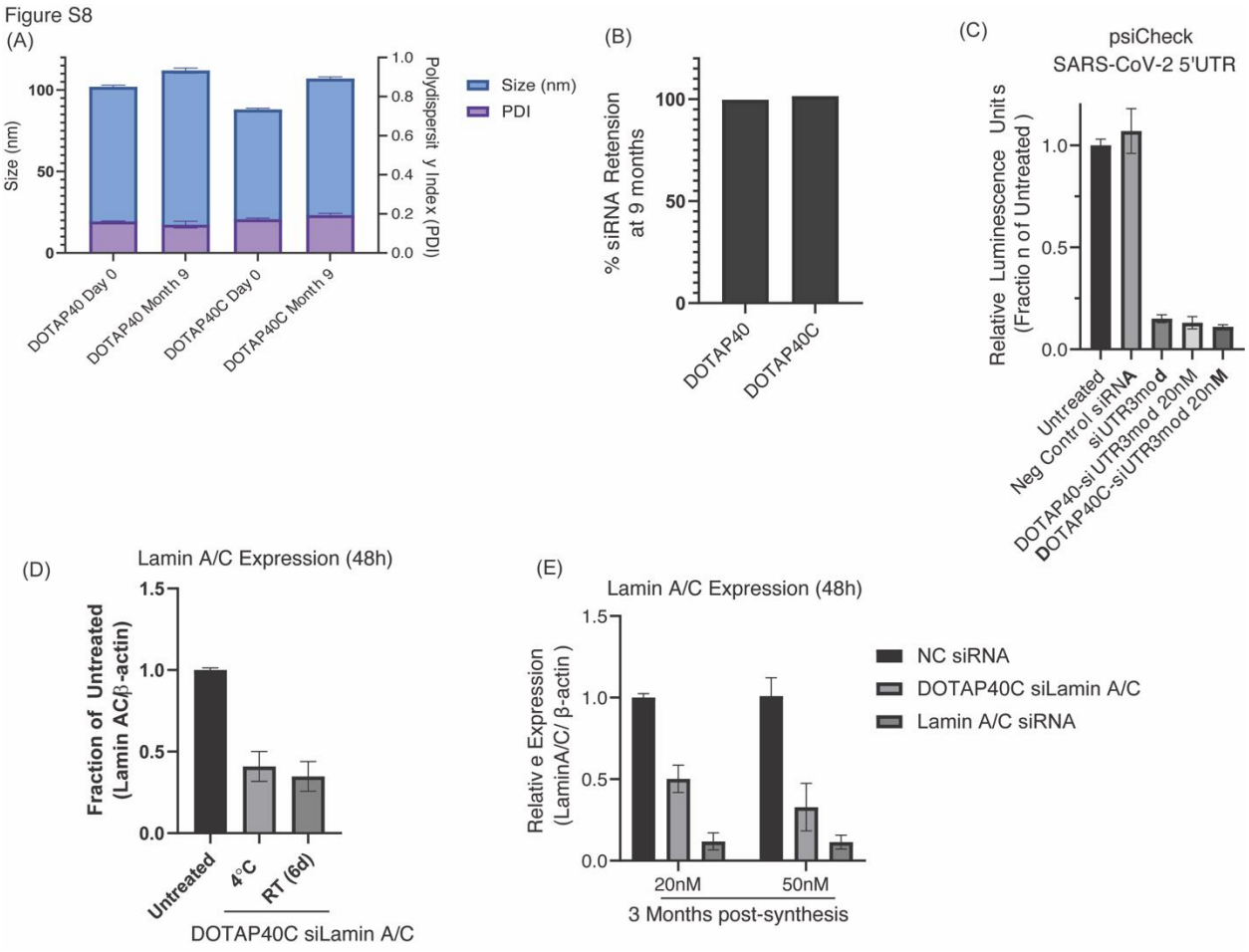

Figure S8 *Stability Evaluation of DOTAP40 and DOTAP40C nanoparticles. (**A**) Size and polydispersity measurements were carried out using dynamic light scattering (DLS) on DOTAP40 and DOTAP40C LNP formulations after synthesis and after 9 months of storage at 4°C. Error bars represent the S.E.M. of 5 runs. (**B**) Retention of siRNAs in LNPs after 9 months of storage. Ribogreen quantification of encapsulated siRNA in LNPs was evaluated at day 0 and again 9 months post synthesis. %siRNA retention= (final encapsulated siRNA concentration)/ (starting encapsulated siRNA concentration) *100. (**C**) DOTAP40 and DOTAP40C LNP-siRNAs containing modified siUTR3 (siUTR3mod) were stored for 9 months at 4°C and subsequently tested for repression of psiCheck SARS-CoV-2 5'UTR reporter via dual luciferase assay at 72 hours post treatment with approximately 20nM LNP-siRNA. Positive and negative control siRNAs were transfected using RNAiMAX. Error bars represent the standard deviation of triplicate wells. (**D**) DOTAP40C LNPs carrying Lamin A/C siRNA were dropped on NIH-3T3 cells at approximately 40nM and incubated for 48 hours. RNA was then extracted and 10ng of RNA was used in a Luna Universal One-Step RT-qPCR (New England BioLabs) to evaluate Lamin A/C expression. Error bars represent the S.E.M of triplicate wells. (**E**) DOTAP40C LNPs carrying Lamin A/C siRNA were stored at 4°C for approximately 3 months and were tested for activity. LNPs were dropped on NIH-3T3 cells at approximately 20 and 50nM and incubated for 48 hours. Positive and negative control siRNAs were transfected using RNAiMAX. Error bars represent the S.E.M of triplicate wells.*

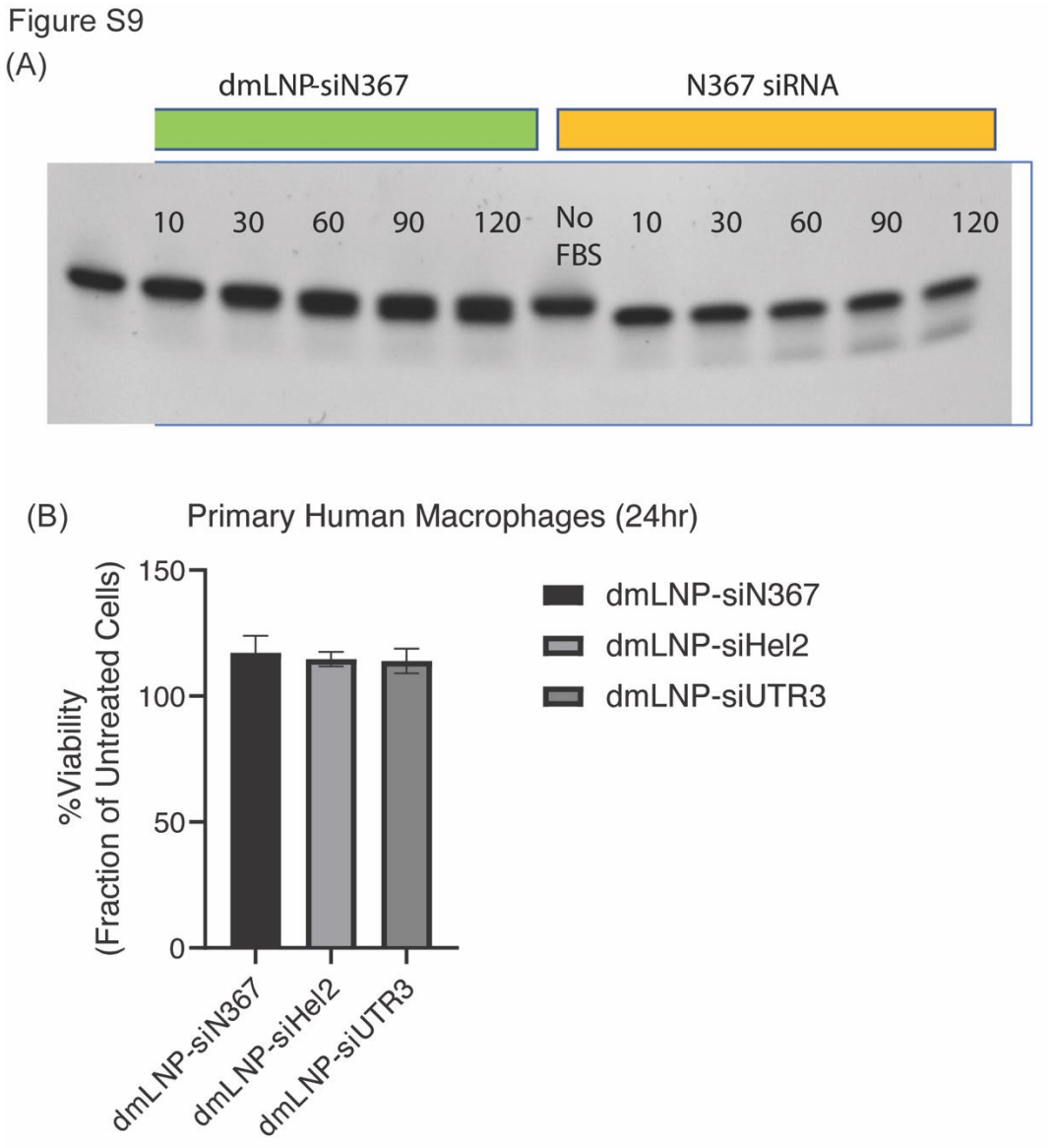

Figure S9 *DmLNP-siRNA serum stability and macrophage viability studies. (**A**) Serum stability evaluation of dmLNP-siRNAs. 2.5ug of dmLNP-siN367 or N367 siRNA alone were incubated in 50ul of FBS (not heat inactivated) at 37°C for 0, 10, 30, 60, 90, and 120 minutes as done in (Wu, 2009 #4497). RNase free water was added up to 200µL and RNA was subsequently extracted using phenol/chloroform (1:1 v/v) and centrifuged for at 14,000 rpm for 10 minutes at 4°C. The aqueous fraction was removed (approximately 25 µL), diluted 1/10, and electrophoresed on a non-denaturing 6% TBE polyacrylamide gel (Novex, Invitrogen) for 30 min at 200V. The gel was then stained with 2 µg/mL EtBr and images were acquired under 254 nm using an EZ Imager (Bio-Rad). Note: dmLNP is the updated name of the DOTAP40C formulation. (**B**) Primary human macrophages were cultured in the presence of approximately 10nM of dmLNP siRNAs and viability was evaluated at 24 hours using an alamarBlue assay. Error bars represent the standard deviation of triplicate wells.*

Table S1 *dsiRNA and siRNA sequences used in this study*

siRNA	RNA sequence sense (5'-3')	RNA sequence antisense (5'-3')
SiRdRp1	rUrArUrGrGrGrUrUrGrGrGrArUrUrArUrCrCrUrArArArUGT	rArCrArUrUrUrArGrGrArUrArArUrCrCrCrArArCrCrCrArUrArArG
SiRdRp1b	rUrArUrGrGrGrUrUrGrGrGrArUrUrArCrCrCrUrArArArUGT	rArCrArUrUrUrArGrGrGrUrArArUrCrCrCrArArCrCrCrArUrArArG
SiRdRp4	rCrArArArGrArArUrArGrArGrCrUrCrGrCrArCrCrGrUrAGC	rGrCrUrArCrGrGrUrGrCrGrArGrCrUrCrUrArUrUrCrUrUrUrGrCrA
SiHel1	rUrGrUrUrGrArUrUrCrArUrCrArCrArGrGrGrCrUrCrArGAA	rUrUrCrUrGrArGrCrCrCrUrGrUrGrArUrGrArArUrCrArArCrArGrU
SiHel2	rArCrCrUrUrArUrArArUrUrCrArCrArGrArArUrGrCrUrGUA	rUrArCrArGrCrArUrUrCrUrGrUrGrArArUrUrArUrArArGrGrUrGrA
SiUTR1	rGrUrCrCrCrUrGrGrUrUrUrCrArArCrGrArGrArArArCAC	rGrUrGrUrUrUrUrCrUrCrGrUrUrGrArArArCrCrArGrGrGrArCrArA
SiUTR3	rArUrArCrCrUrUrCrCrCrArGrGrUrArArCrArArArCrCrAAC	rGrUrUrGrGrUrUrUrGrUrUrArCrCrUrGrGrGrArArGrGrUrArUrArA
siUC1	rArArCrUrUrArUrGrUrArCrUrCrArUrUrCrGrUrUrU	rArCrGrArArUrGrArGrUrArCrArUrArArGrUrUrCrG
siUC2	rArCrUrUrArUrGrUrArCrUrCrArUrUrCrGrUrUrUrC	rArArCrGrArArUrGrArGrUrArCrArUrArArGrUrUrC
siUC3	rUrUrUrGrArArUrGrUrGrGrCrUrArArArUrCrUrGrA	rArGrArUrUrUrArGrCrCrArCrArUrUrCrArArArGrA
siUC4	rArCrCrArCrCrUrUrGrUrArGrGrUrUrUrGrUrUrArC	rArArCrArArArCrCrUrArCrArArGrGrUrGrGrUrUrC
siUC5	rUrGrGrArArCrCrArCrCrUrUrGrUrArGrGrUrUrUrG	rArArCrCrUrArCrArArGrGrUrGrGrUrUrCrCrArGrU
siUC6	rArArCrCrArCrCrUrUrGrUrArGrGrUrUrUrGrUrUrA	rArCrArArArCrCrUrArCrArArGrGrUrGrGrUrUrCrC
siUC7	rUrGrGrArCrUrGrArGrArCrUrGrArCrCrUrUrArCrU	rUrArArGrGrUrCrArGrUrCrUrCrArGrUrCrCrArArC
siUC8	rArCrUrGrGrArArCrCrArCrCrUrUrGrUrArGrGrUrU	rCrCrUrArCrArArGrGrUrGrGrUrUrCrCrArGrUrUrC
siUC9	rArUrGrArUrGrArUrUrArUrUrUrCrArArUrArArArA	rUrUrArUrUrGrArArArUrArArUrCrArUrCrArUrCrA

siUC10	rArCrUrArUrArUrGrUrUrArArArCrCrArGrGrUrGrG	rArCrCrUrGrGrUrUrUrArArCrArUrArUrArGrUrGrA
NC	rCrArUrArUrUrGrCrGrCrGrUrArUrArGrUrCrGrCrG rUrUAG	rCrUrArArCrGrCrGrArCrUrArUrArCrGrCrGrCrArArUrArUrGrGrU
L362	rGrArCrUrUrUrCrCrGrCrUrGrGrGrGrArCrUrUrUrC	rUrGrGrArArArGrUrCrCrCrCrArGrCrGrGrArArArG
N367	rCrUrGrArCrCrUrUrUrGrGrArUrGrGrUrGrCrUrUrC	rUrGrGrArArArGrUrCrCrCrCrArGrCrGrGrArArArG
Lamin A/C	rGrArCrUrUrGrGrUrGrUrGrGrArArGrGrCrGrCrArGrArACA	rUrGrUrUrCrUrGrCrGrCrCrUrUrCrCrArCrArCrCrArArGrUrCrArG

RNA bases denoted with r; DNA bases are capitalized

Table S2 *Normalised immune gene expression from the unsupervised hierarchical cluster analysis.*

Table S3 *Normalised immune gene expression from the unsupervised hierarchical cluster analysis from day 6 volcano plot data in Figure S6.*

Materials and Methods:

Lipids/Reagents:

The following lipids 1,2-dioleoyl-3-trimethylammonium-propane (DOTAP), 1,2-distearoyl-sn-glycero-3-phosphocholine (DSPC), Cholesterol, N-palmitoyl-sphingosine-1-{succinyl[methoxy(polyethylene glycol)2000]} (C16 PEG2000 Ceramide) were purchased from Avanti Polar Lipids (Alabaster, AL, USA). DLin-MC3-DMA was purchased from (MedChemExpress; Monmouth Junction, NJ, USA). All lipids were dissolved in ethanol and aliquoted in amber glass vials. Lipophilic dye DiL (DilC_{18}(3) or DiD (DilC_{18}(5) (1,1'-dioctadecyl-3,3,3',3'-tetramethylindocarbocyanine perchlorate) at 1mM stock in ethanol(Invitrogen; Carlsbad, CA, USA) was used to label nanoparticles at 0.5µM for biodistribution studies.

dmLNP Synthesis:

Lipids were prepared at a 40:25:10:22:3 (DOTAP:MC3:DSPC:Chol:PEG) molar ratio. Lipids in ethanol were mixed with nucleic acids in an aqueous phase at a mol cationic lipid: mol RNA (N:P) ratio of 3:1 using the NanoAssemblr Benchtop machine (Precision NanoSystems; Vancouver, BC, Canada). This machine contains a microfluidic chip by which the injected lipids and nucleic acids are mixed rapidly in a staggered herringbone pattern at a total flow rate of 12mLl/min. The controlled mixing of the aqueous and organic streams produces homogeneous nanoparticles. Immediately following the mixing process, the nanoparticles were diluted 1:4 with 1XPBS to reduce the amount of ethanol present in solution. The nanoparticle solution was further diluted with 1XPBS up to 15 mL and then concentrated using a 10 kDa Amicon ultra-15 filter (Millipore; Burlington, MA, USA) via centrifugation at 2,000 x G for 30 minutes. The flow through was discarded and another 15 mL 1XPBS was added to the column and centrifuged at 2,000 x G for 40 mins. The concentrated nanoparticles were then pushed through a 0.22µm filter and stored at 4°C.

Characterization of dmLNPs:
Nanoparticles were analyzed using dynamic light scattering (DLS) to determine polydispersity (PDI) and surface charge was determined by measuring zeta potential on a ZetaPals (Brookhaven Instruments Corporation; Holtsville, NY, USA). Concentration and relative nanoparticle size was determined using nanoparticle tracking analysis (NTA) on the Nanosight (NS300) (Malvern Panalytical; Malvern, UK) and the qNANO Gold (IZON; Christchurch, New Zealand). For the NTA, samples were diluted 10,000X in PBS and samples measured in triplicate technical replicates. A blue 488 laser was used to detect the LNPs, with a slide shutter level set to 1200X and the slider gain set to 146Y, and the syringe pump speed set to 30 using a flow-cell top plate module. For the qNano, a NP150 nanopore (iZON; Christchurch, New Zealand) was used to measure the LNPs. LNPs were diluted 40X in measuring solution [2] measured at 2 different pressures. Concentration was determined by measuring calibration beads at known concentrations and extrapolating particles/mL for each sample evaluated using the iZON control suite software (V3.4.2.48).

To measure the amount of siRNA encapsulated inside the nanoparticles the Quant-IT Ribogreen assay was carried out (Molecular Probes; Eugene, OR, USA). The standard protocol was modified to include a 15 minute, 37°C incubation of the nanoparticles in the presence of 2% Triton to facilitate release of the encapsulated nucleic acids. %encapsulation = (siRNA-LNP in 2%Triton - siRNA-LNP in TE)/siRNA-LNP in 2%Triton-X100 based on [3].

siRNAs:
siRNAs or dsiRNAs targeted to SARS-CoV-2 were ordered from Integrated DNA Technologies (Coralville, IA, USA) as duplexed RNA. Target sequences for siRNAs are listed in Table S1. The negative control (NC) dsiRNA was purchased from IDT. Control siRNAs, N367 and L362 were designed towards the miRNA-N367 target site [4-6] and the 5'LTR [7,8] of HIV-1 respectively, and were synthesized as duplexed RNA by IDT. Sequences for all dsiRNAs and siRNAs employed in this study are in supplementary Table 1. The modUTR3 was designed as per supplementary Figure S2 and synthesized by IDT as an RNA duplex. HPLC purified and high quantity dsiRNAs and siRNAs, UTR3, Hel2, UC7, N367 were synthesized by the RNA/DNA Synthesis core at the City of Hope (Duarte, CA) and used in the *in vivo* experiments.

Cells:
HEK293 cells were purchased from ATCC (CRL-1573) and cultured in DMEM with 10% fetal bovine serum (FBS) at 37°C and 5% CO_2. Vero E6 cells were obtained from ATCC. Vero E6 and HEK293 cells were maintained in complete media; DMEM (Gibco-Invitrogen, Waltham, MA) supplemented with 10% heat inactivated foetal bovine serum (FBS) (30 min at 56°C, Gibco-Invitrogen, Waltham, MA) and 1% of antibiotic/glutamine preparation (100 U/ml penicillin G, 100 U/ml streptomycin sulphate, and 2.9 mg/ml of L-glutamine) (Gibco-Invitrogen, Waltham, MA). THP1-Dual™ cells (InvivoGen) were grown in RPMI 1640, 2 mM L-glutamine, 25 mM HEPES, 10% heat-inactivated FBS , 100 μg/ml Normocin™ and Pen-Strep (100 U/ml-100 μg/ml). NIH-3T3 cells were obtained from ATCC (CRL-1658) and cultured in DMEM with 10% FBS and H1299 cells were obtained from ATCC (CRL-5803) and cultured in RPMI with 10% FBS and cultured at 37°C and 5% CO2.

Virus cultivation:
SARS-CoV-2 VIC1 strain was obtained from the Peter Doherty Institute for Infection and Immunity and Melbourne Health, Victoria, Australia [9] and cultured in Vero E6 cells. Viral supernatant was concentrated in Amicon ® Ultra-15 Centrifugal Filter units (Merck, Germany) and viral titre determined by the viral immunoplaque assay as previously described [10].

Cell transfection and siRNA Screening:
Cells were seeded overnight in a 12-well plate to 70-80% confluency before transfecting siRNAs with either FuGENE 6 (Promega, Madison, WI) or Lipofectamine 2000 (Gibco-Invitrogen, Waltham, MA) in OptiMEM (Gibco-Invitrogen, Waltham, MA) as per manufacturer's protocol. For the knockdown reporter assays, the CoV-2 ORF, helicase, 5'UTR) were cloned downstream of *Renilla* luciferase in a pSI-CHECK reporter vector and transfected with the siRNA into HEK293 in a 48-well plate. At 48 hrs post-transfection the levels of luciferase were measured and made relative to a control siRNA set at 100%. 250ng of pSI-CHECK plasmids and 0.75, 7.5 or 75 pmol of siRNA was used. Luciferase reporter activity was measured using a Dual-Luciferase® Reporter Assay System and measured on a GloMax Explorer microplate reader (Promega; Madison, WI, USA).

Immunostimulation assay:
THP1-Dual™ cell IRF and NFkB reporter gene expression were measured as per manufacturer's protocol (InvivoGen). NF-kB and IRF activation pathways were measured by assessing the activity of alkaline phosphatase and luciferase. 2'3'-cGAMP and LPS were obtained from InvivoGen (San Diego, CA).

Negative staining electron microscopy:
Nanoparticles diluted 1/100 in 1X PBS were absorbed to glow-discharged, carbon-coated 200 mesh EM grids. Samples were prepared by conventional negative staining with 1% (w/v) uranyl acetate. Electron microscopy images were taken on an FEI Tecnai 12 transmission electron microscope equipped with a Gatan OneView CMOS camera. Images were analyzed using ImageJ software (V1.52d).

dmLNP-siRNA uptake evaluation in vivo:
All animal experiments were approved by the City of Hope IACUC (20025). To determine if siRNA loaded nanoparticles show preferential lung accumulation, we injected C57/BL6 mice IV with DiD-labeled nanoparticles at 1mg/kg siRNA dose. 24 hours after injection, mice were euthanized and the lung, liver, and spleen were removed. Organs were imaged for DiD fluorescence using a LagoX imager (Spectral Instruments Imaging, AZ) at an excitation and emission wavelength of 640 and 690 nm, respectively.

Long-term stability:
To determine the long-term stability of our LNPs we evaluated size and polydispersity using DLS and monitored siRNA encapsulation at 9 months post-formulation.

SARS-CoV-2 in vivo infection model:
K18-hACE2 mice were purchased from the Jackson Laboratory (Bar Harbor, ME) and bred in-house at the Griffith University Animal Resource Center. Mice were intranasally infected with 1-

4 x 10^4 PFU (20 µL total volume) of live SARS-CoV-2 while under isoflurane anesthesia. Mice were subsequently treated with either LNP or DOTAP 40 complexed siRNAs, 5% sucrose (for LNP control) or PBS (for DOTAP 40 control) vehicle control (retro-orbitally) while under isoflurane anesthesia. Mice were monitored daily for weighing and clinical scoring. This work was conducted in a BSL3 approved animal facility at Griffith University (Animal ethics approval: MHIQ/07/20/AEC).

Viral plaque and immunoplaque assay:
For viral plaque assays, Vero E6 cells were infected with a MOI 0.002 of SARS-CoV-2 for 1hr before overlaying with 1% methylcellulose- viscosity 4,000 centipoise (Sigma- Aldrich, St. Louis, MO). Cells were incubated for 4 days at 37°C before fixing in 8% formaldehyde and stained with 1% crystal violet to visualize plaques. Viral immunoplaque assays were performed on Vero E6 cells as described previously [10] using recombinant monoclonal antibodies that recognize SARS-CoV-2 (CR3022). Antibodies were obtained from Dr Naphak Modhiran and A/Prof. Dan Watterson (School of Chemistry and Molecular Biosciences, The University of Queensland, QLD, Australia). Virus titers were denoted as plaque forming units (PFU)/milliliter or PFU/grams of tissue.

Viral copy number determination:
To determine viral copy numbers in organ tissues, digital PCR against the N gene (CDC primers from IDT - SARS-CoV-2 N1) was performed in Quant-Studio 3D Digital PCR 20K chips (Thermo Scientific, Waltham, MA) ona ProFlex 2×Flat Block Thermal Cycler (Thermo Scientific, Waltham, MA). Results are analyzed on the QuantStudio 3D AnalysisSuite software (Thermo Scientific, Waltham, MA) and expressed as viral copies per gram of tissue.

qRTPCR and gene expression analysis:
To evaluate the *in vitro* activity of LNPs carrying Lamin A/C siRNA, RT-qPCR analysis was carried out. Briefly, approximately 25,000 NIH-3T3 cells were seeded in a 24-well plate and LNPs were added at indicated concentrations. Positive and negative control siRNAs were transfected using lipofectamine RNAiMAX (Gibco-Invitrogen, Waltham, MA) in OptiMEM (Gibco-Invitrogen, Waltham, MA) following the manufacturer's protocol. 48 hours after treatment, RNA was isolated using the Maxwell RSC purification kit (Promega; Madison, WI, USA). A total of 10ng of RNA was used in Luna Universal One-Step RT-qPCR analysis (NEB; Ipswich, MA, USA) for Lamin A/C (5'-GAGAGGCTAAGAAGCAGC-3' and 5'-ACGCAGTTCCTCGCTGTAA-3'and β-actin 5'-GCTACAGCTTCACCACCACA-3' and 5'-TCTCCAGGGAGGAAGAGGAT-3'genes using the LightCycler96 real-time PCR system (Roche; Basel, Switzerland). Cycling conditions were as follows: reverse transcription (55°C for 10 min) and initial denaturation (95°C for 1 min) followed by 40 cycles of denaturation (95°C for 10 sec) and extension (60°C for 30 sec, with plate read). The fold change in gene expression was determined using the 2-DDCt method. The following qPCR primers were purchased from IDT.

dmLNP-siRNA psi-Check assay:

To analyse in vitro activity of dmLNP-siUTR3 which targets the 5'UTR of SARS-CoV-2 we utilized the psi-Check-5'UTR reporter plasmid. Briefly, 20,000 H1299 cells were reverse transfected using 100ng of psi-Check-5'UTR plasmid using Lipofectamine 2000 (Gibco-

Invitrogen, Waltham, MA) in OptiMEM (Gibco-Invitrogen, Waltham, MA) as per manufacturer's protocol. After 24 hours, dmLNP-siRNAs were dropped on cells using equal volumes of OptiMEM. 72 hours after dmLNP addition, luciferase reporter activity was measured using a Dual-Luciferase® Reporter Assay System and measured on a GloMax Explorer microplate reader (Promega; Madison, WI, USA).

Macrophage viability study:

Monocytes were collected from whole blood and stimulated with 10 ng/mL of granulocyte-macrophage colony-stimulating factor (GMCSF) for 6 days to form macrophages primed for a type 1 immune response [11]. A total of 100,000 macrophages were seeded and dosed with approximately 10nM dmLNP siRNAs for 24 hours. The alamar blue viability assay was performed following the manufacturer's protocol. Following a 1 hr incubation at 37C, fluorescence was measured on a GloMax Explorer microplate reader (Promega; Madison, WI, USA). Blank media readings were subtracted from all experimental values.

NanoString gene expression analysis:
Immune gene expression analysis was undertaken using the NanoString nCounter analysis system (NanoString Technologies, Seattle, WA) and the commercially available nCounter Mouse PanCancer Immune Profiling panel kit. The PanCancer Immune profiling panel contains 730 genes of key inflammatory pathways 40 reference/housekeeping genes. The nCounter system directly detects and counts single-stranded nucleic acid via reporter probes affixed with fluorophore barcodes and biotinylated capture-probes attached to microscopic beads. Probes are then affixed to lanes in cartridges and read in a digital scanner. Following the manufacturer's protocol, 100 ng of total RNA extracted from tissue was hybridised with probes at 65 °C for 20 hours before being inserted into NanoString Prep Station where the target-probe complex was immobilised onto the analysis cartridge. Cartridges were read by the nCounter Digital Analyser for digital counting of molecular barcodes corresponding to each target at 555 fields of view.

Nanostring Data analysis:
Gene expression data was analysed using a combination of the Advanced Analysis Module in the nSolver™ Analysis Software version 4.0 from NanoString Technologies (NanoString Technologies, WA, USA), TIGR Multi-Experiment Viewer (http://mev.tm4.org) or the Limma package in the R Statistical Computing Environment. nSolver enables quality control (QC), normalisation, differential gene expression (DGE), Pathview Plots and immune cell profiling. Negative and positive controls included in probe sets were used for background thresholding, and normalizing samples for differences in hybridization or sample input respectively. Data was corrected for input volume via internal housekeeping genes using the geNorm algorithm. Genes that were expressed below 20 counts in more than 90% of samples were excluded from analysis. Differential gene expression between the treatment groups was determined using a variance stabilised t-test. Pathway analysis was undertaken using the Kyoto Encyclopedia of Genes and Genomes (KEGG).

*Statistical analysis:*All statistical analyses were performed using the statistical software package GraphPad Prism 9 and described in detail in respective figure legends.

Literature cited:

1. Gibbs, R.A., Weinstock, G.M., Metzker, M.L., Muzny, D.M., Sodergren, E.J., Scherer, S., Scott, G., Steffen, D., Worley, K.C., Burch, P.E., Okwuonu, G., et al. (2004). Genome sequence of the Brown Norway rat yields insights into mammalian evolution. Nature *428*, 493-521.
2. Liang, M., Morizono, K., Pariente, N., Kamata, M., Lee, B., and Chen, I.S. (2009). Targeted transduction via CD4 by a lentiviral vector uses a clathrin-mediated entry pathway. J Virol *83*, 13026-13031. 10.1128/JVI.01530-09.
3. Leung, A.K., Hafez, I.M., Baoukina, S., Belliveau, N.M., Zhigaltsev, I.V., Afshinmanesh, E., Tieleman, D.P., Hansen, C.L., Hope, M.J., and Cullis, P.R. (2012). Lipid Nanoparticles Containing siRNA Synthesized by Microfluidic Mixing Exhibit an Electron-Dense Nanostructured Core. J Phys Chem C Nanomater Interfaces *116*, 18440-18450. 10.1021/jp303267y.
4. You, X., Zhang, Z., Fan, J., Cui, Z., and Zhang, X.E. (2012). Functionally orthologous viral and cellular microRNAs studied by a novel dual-fluorescent reporter system. PLoS One *7*, e36157. 10.1371/journal.pone.0036157.
5. Omoto, S., and Fujii, Y.R. (2005). Regulation of human immunodeficiency virus 1 transcription by nef microRNA. J Gen Virol *86*, 751-755. 10.1099/vir.0.80449-0.
6. Omoto, S., and Fujii, Y.R. (2006). Cloning and detection of HIV-1-encoded microRNA. Methods Mol Biol *342*, 255-265. 10.1385/1-59745-123-1:255.
7. Turner, A.M., Ackley, A.M., Matrone, M.A., and Morris, K.V. (2012). Characterization of an HIV-targeted transcriptional gene-silencing RNA in primary cells. Hum Gene Ther *23*, 473-483. 10.1089/hum.2011.165.
8. Weinberg, M.S., Villeneuve, L.M., Ehsani, A., Amarzguioui, M., Aagaard, L., Chen, Z.X., Riggs, A.D., Rossi, J.J., and Morris, K.V. (2006). The antisense strand of small interfering RNAs directs histone methylation and transcriptional gene silencing in human cells. RNA *12*, 256-262. 10.1261/rna.2235106.
9. Caly, L., Druce, J., Roberts, J., Bond, K., Tran, T., Kostecki, R., Yoga, Y., Naughton, W., Taiaroa, G., Seemann, T., Schultz, M.B., et al. (2020). Isolation and rapid sharing of the 2019 novel coronavirus (SARS-CoV-2) from the first patient diagnosed with COVID-19 in Australia. Med J Aust *212*, 459-462. 10.5694/mja2.50569.
10. Amarilla, A.A., Modhiran, N., Setoh, Y.X., Peng, N.Y.G., Sng, J.D.J., Liang, B., McMillan, C.L.D., Freney, M.E., Cheung, S.T.M., Chappell, K.J., Khromykh, A.A., et al. (2021). An Optimized High-Throughput Immuno-Plaque Assay for SARS-CoV-2. Front Microbiol *12*, 625136. 10.3389/fmicb.2021.625136.
11. Menck, K., Behme, D., Pantke, M., Reiling, N., Binder, C., Pukrop, T., and Klemm, F. (2014). Isolation of human monocytes by double gradient centrifugation and their differentiation to macrophages in teflon-coated cell culture bags. J Vis Exp, e51554. 10.3791/51554.